

ABSTRACT

Title of Document

FABRICATION OF BRAGG GRATINGS
USING INTERFEROMETRIC LITHOGRAPHY

Ricardo A. Pizarro, Master of Science, 2007

Directed By:

Professor Julius Goldhar
Department of Electrical and Computer
Engineering

A setup has been designed and realized for the fabrication of Bragg Gratings in edge emitting semiconductor laser. In this setup a HeCd laser ($\lambda=325\text{nm}$) is used in a Lloyd's mirror configuration, to interferometrically expose a sinusoidal grating on photoresist. The dilution of photo-resistant (PR) material allows for a spincoat thickness of 50nm which is needed to minimize standing waves in the photo-resist that lead to a nonuniform exposure. Variations of exposure time show the progression of photo-resist gratings. Etching recipes using both dry and wet etching techniques were successfully used to transfer the grating pattern into semiconductor material. Bragg Gratings with $\Lambda=250\text{nm}$ in InP and InGaAs have been characterized with an Atomic Force Microscope to have a grating height of over 100nm.

FABRICATION OF BRAGG GRATINGS USING INTERFEROMETRIC
LITHOGRAPHY

By

Ricardo Andres Pizarro

Thesis submitted to the Faculty of the Graduate School of the
University of Maryland, College Park, in partial fulfillment
of the requirements for the degree of
Master of Science
2007

Advisory Committee
Professor Julius Goldhar, Chair
Dr. Thomas E. Murphy
Dr. Christopher J. K. Richardson

© Copyright by
Ricardo Andres Pizarro
2007

Acknowledgements

First and foremost, I would like to thank my advisor Julius Goldhar. Without his help I would not have gotten the opportunity to work in such a wonderful facility or with such smart and motivated individuals. I have learned a great deal from him during his lectures, in the lab, and even outside work playing tennis. His great personality makes it quite easy to work with him. I feel lucky to have him as my advisor.

Dr. Christopher Richardson has also in a way played the role of my advisor. I have been very fortunate to work with him on this project and learn so much from him. His motivation, organization, and dedication are but a few qualities of his that inspire me to model my work after him.

I have also been fortunate to take classes from the talented Dr. Thomas Murphy. Not only have I learned a great deal from his lectures, but his previous work has helped me to understand mine. The encounters I have had with him, have always been helpful in terms of the progress of my work.

Anna Tauke-Pedretti's summer visit last year was a great catalyst to getting this project off the ground. Without her help, the setup would have been built as quickly as it was. She showed me much inside the cleanroom, how to use the AFM, and other important skills used every day in the lab.

Everyone at LPS, the facility where I work, has been most helpful as well. Particularly, Victor Yun, and Yongzhang Leng who have continuously helped me with the mechanics and the theory of the setup I built. Les from the machine shop has patiently fulfilled all my demands in terms of building me parts I need. Greg Latini and Mark Thornton are always very helpful with computers.

All those in the Cleanroom with their consistent support have made it easy to work inside. Toby Olver, Steve Brown, Sean Flannery, Lisa Lucas who have all trained me, answered questions, given me a hand. George de la Vergne has been quite interested in sharing stories about mate, futbol (soccer), and any topic of interest.

Dan Hinkel and Arun Mamphazy were both very helpful with the SEM. Michael Dreyer and Taesoon Kwon have both been very helpful to accurately and consistently make AFM scans.

The MBE group and their meetings who I have been most fortunate to be a part of have also helped tirelessly. I particularly like to thank Kanakaraju Subramaniam, Lei He, and Joseph Di Pasquale III, for their help with papers, pictures, and beers.

I would particularly like to thank all those who have not only helped me with lab-work and class-work but have taken the time to become a friend of mine. Such characters like Arthur Liu, Dyan Ali, Shuo-yen Tseng, Ehren, Younggu Kim, Donghun (papadong) Park, David Park, and Glenn Hutchinson are simply irreplaceable. With them I have shared many memories playing tennis, basketball, eating, running errands, getting coffee.

Finally, I would like to thank my family who has given me everything that I am. My father inspired me to reach for my dreams and told me that I could be whatever I wanted to be. My mother's endless source of love has been very supportive during rough times. My brothers and sisters with whom I have shared so many memories have been a big help emotionally as well.

Table of Contents

Chapter 1: Introduction/Motivation.....	1
Chapter 2: Theory	3
2.1. Bragg Gratings	3
2.1.1. Introduction.....	3
2.1.2. Periodic Waveguide	5
2.1.3. Effective Index Method for DBR laser	10
2.1.4. Finite Length Gratings	23
2.2. Standing Wave	25
2.2.1. Interference of Light	25
2.2.2. Unwanted Standing Wave.....	28
Chapter 3: Experimental Setup / Design.....	31
3.1. Lloyd's Mirror Setup.....	31
3.2. Propagating a Gaussian	33
3.2.1. Laser Cavity	35
3.2.2. Aperture to Lens	37
3.2.3. Lens to Lloyd's Mirror.....	39
3.2.4. Pinhole size	41
3.3. Mirror	44
3.3.1. Aligning Lloyd's Mirror	44
3.3.2. Angle Calibration.....	45
3.3.3. Range of angles.....	47

3.4. Variation across Sample	49
3.4.1. Intensity of Electric Field.....	49
3.4.2. Grating Period.....	51
3.5. Grating Period Measurement	53
3.5.1. Alternate Setup.....	53
3.5.2. Limit to Grating Measurement.....	56
3.5.3. Making a measurement	56
Chapter 4: Fabrication	59
4.1. Preparing the Sample	59
4.2. Exposing Positive Resist using Lloyd's Mirror	62
4.2.1. Turning the Laser On	62
4.2.2. Loading the Sample	63
4.2.3. Getting Flat Bottoms.....	63
4.3. Etching Gratings into Semiconductor.....	69
Chapter 5: Conclusion	77
Appendix A – Processing Recipes I.....	79
Appendix B – Processing Recipes II	81
Appendix C –Operating the HeCd Laser	83
Appendix D - Matlab Code.....	84
References	85

Chapter 1: Introduction/Motivation

As we head into the future, technology will keep getting better, faster, and more cost-effective. Instead of sending an electrical signal through a copper wire, messages will be relayed by laser signals through waveguide material, like optical fibers. As this change begins to take place, electrical components will need to be replaced by optical ones.

One of the components that have been designed and studied for some time now is called Bragg Gratings. This component can serve as a building block to manufacture optical filters and laser structures, namely Distributed Feedback (DFB) and Distributed Bragg Reflectors (DBR). In turn these laser structures can be implemented in semiconductors to further explore other devices.

DBR lasers have been successfully implemented with two “sampled grating” mirrors with 57nm nonthermal tuning at a $1.475\mu\text{m}$ wavelength [1]. To this widely tunable laser it has been reported that an Electroabsorption Modulator can be successfully integrated [2]. Also a Semiconductor Optical Amplifier has been successfully integrated with the laser and its characteristics examined [3].

A successful fabrication of a high performance laser has been reported with the successful implementation of this DFB technology [4]. In another experiment by utilizing GaInNAs active-layer material and lateral DFB, singlemode emission has been realized at $1.5\mu\text{m}$ [5]. Also Wavelength-Selectable Lasers have been implemented by the use of DBR technology for realizing fast tunable lasers that can cover a wide range of wavelengths [6]. Even a wavelength-tunable *organic* solid state laser based on 2nd order DFB has been reported [7].

These are just a few of many successful implementations that can be realized with a DBR or DFB laser. The advantage of having Bragg reflectors behave as mirrors in the lasing cavity is the tuning range it offers. There exist even more successful implementations of Bragg Gratings in semiconductor not mentioned here. By having the ability to make such devices we will be able to study some of these laser structures mentioned.

The main goal behind the research presented in this thesis is to design and realize a robust setup where Bragg Gratings could be made at the telecommunication frequency. If another scientist can use this thesis as guide to either use the setup built or design a different one altogether then it has been successful. This thesis is broken down into three subsequent chapters and the conclusion where all the results are summarized.

Chapter 2 covers the theory behind two important topics of this project. The first part discusses how Bragg Gratings on a waveguide cause a signal traveling in the forward direction to be partly reflected and partly transmitted. The latter part details how the pattern needed to make gratings is realized by the interferences of two plane waves.

In chapter 3, the groundwork for building such a robust setup is detailed. It begins by discussing the implementation of the Lloyd's Mirror to create the interference pattern on positive resist. Then the path traveled by the Gaussian beam is examined in detail to ensure proper UV exposure of the sample. Finally an added feature of the setup is presented as a way to measure the period of the gratings fabricated.

Chapter 4 covers the process used for the fabrication and presents results achieved by setup realized. The different steps of the process are discussed and studied in order to determine the best recipe for consistent, reproducible results.

Chapter 2: Theory

This chapter discusses two essential subjects for this experiment to be realized. The first analyzes how Bragg Gratings cause a signal to be reflected as it is traveling down the waveguide. The grating period needed as calculated in the following section is 244.5nm making the fabrication out of reach of conventional lithography. In the preceding section, the interference of two plane waves is discussed that will create a standing wave at the period calculated.

2.1. Bragg Gratings

2.1.1. Introduction

The system to be studied in this section is a waveguide with gratings on top depicted in Figure 2.1. Gratings can be thought of as a waveguide material with a sinusoidal pattern corrugated on top. With the proper dimensions, a signal within a certain frequency bandwidth traveling down the waveguide will get reflected.

A signal will diffract in the reverse direction when the Bragg Condition is met. That is, reflections from subsequent periods of the grating have to interfere constructively. This is analogous to when a signal is reflected off a dielectric stack mirror. The Bragg condition for an p^{th} -order Bragg grating as defined later is:

$$\Lambda = \frac{p\lambda}{2\bar{n}} \quad (2.1)$$

where λ is the wavelength of the signal in free space, \bar{n} the effective index of refraction of the waveguide, and Λ the fundamental period of the grating. Only the first diffracted order ($p=1$) is considered in this thesis, since it causes the strongest diffraction.

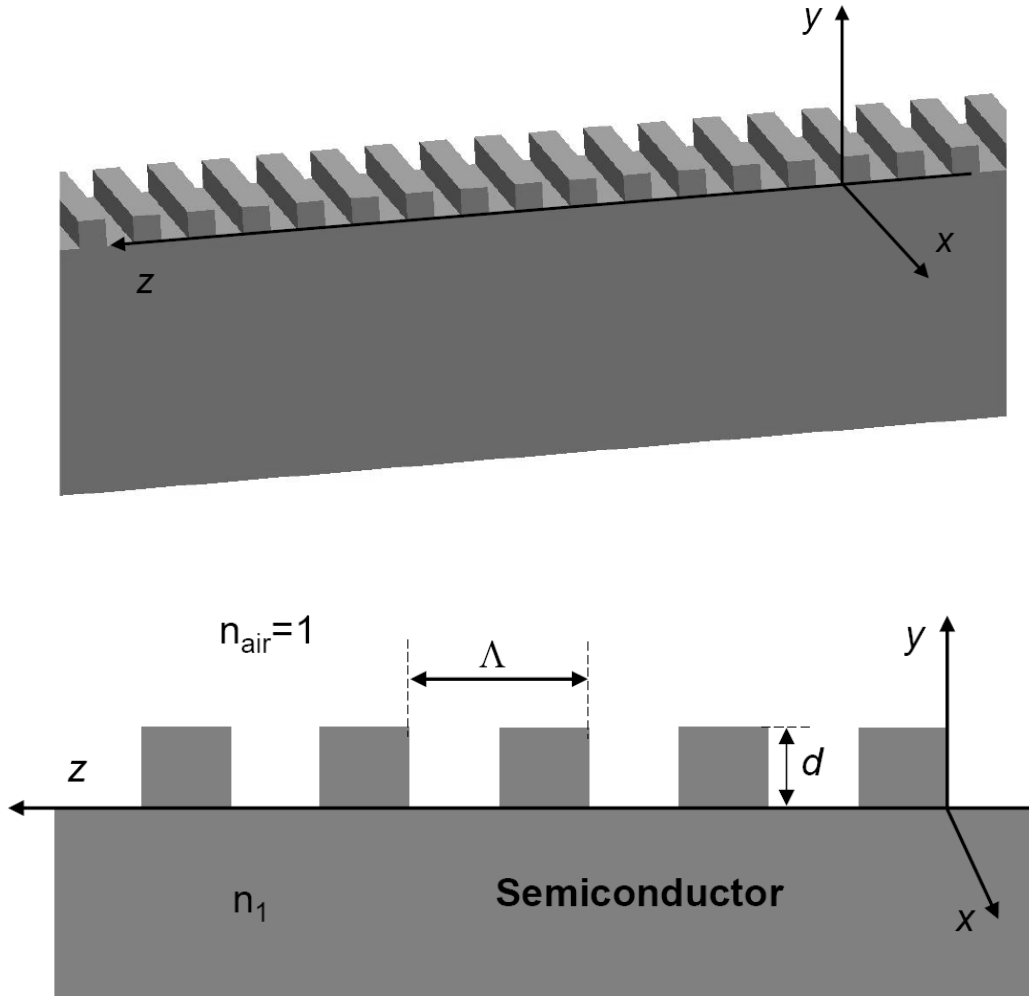


Figure 2.1: 3D and 2D view of Bragg Gratings on top of a waveguide material. The Bragg Gratings studied here can be thought of as a corrugated square wave on top of the waveguide. Dimensions specified are used in analysis of the gratings.

Assuming a working wavelength of 1550nm, the period needed can be calculated if we know the refractive index of the material used. The semiconductor used in this experiment, Indium Phosphide, has an average index of refraction of 3.17 measured by [8]. This translates to a grating period of $\Lambda = (1*1550nm)/(2*3.17) = 244.5nm$

2.1.2. Periodic Waveguide

There are different approaches used to study the behavior of gratings as different modes propagate down a waveguide. Here we consider the gratings as periodic index perturbations in the waveguide in a similar analysis to both [9, 10].

We begin the analysis from the well-known wave equation written as

$$\nabla^2 \bar{E}(\vec{r}, t) = \mu \varepsilon_{eff}(\vec{r}) \frac{\partial^2 \bar{E}(\vec{r}, t)}{\partial t^2} \quad (2.2)$$

where $\varepsilon_{eff}(\vec{r}) = \varepsilon(\vec{r}) + \Delta\varepsilon(\vec{r})$ is the effective dielectric constant. The latter part of this dielectric constant can be thought of as a perturbation to the waveguide. In the following section it will be shown that the physical corrugation can directly determine $\Delta\varepsilon$. That is the physical corrugation on top of the waveguide will be defined as $\Delta\varepsilon(\vec{r}) \equiv \varepsilon_0 \Delta n^2(\vec{r})$.

The effective dielectric does not vary with time and so we can plug into Eq.2.2 to get

$$\nabla^2 \bar{E}(\vec{r}, t) - \mu \varepsilon(\vec{r}) \frac{\partial^2 \bar{E}(\vec{r}, t)}{\partial t^2} = \mu \varepsilon_0 \Delta n^2(\vec{r}) \frac{\partial^2 \bar{E}(\vec{r}, t)}{\partial t^2} \quad (2.3)$$

The right side of Eq.2.3 is dependent on the corrugation as defined by the perturbation part of the effective dielectric constant. For the sake of generality let's define the electric field as a superposition of the eigenmodes in a waveguide.

$$\vec{E}(\vec{r}, t) = \sum_m U_m(x, y) E_{m0}(z) e^{i(\omega t - \beta_m z)} \quad (2.4)$$

Here the modes have been separated into the propagating direction, z and the transverse direction. U_m is the m^{th} transverse eigenmode that completely satisfies

$$\nabla_T^2 U_m + \omega^2 \mu \epsilon(\vec{r}) U_m - \beta_m^2 U_m = 0 \quad (2.5)$$

Substituting in the definition of the electric field as a superposition of eigenmodes into the left side of Eq.2.3 will give us

$$\underbrace{\nabla^2 \sum_m U_m E_{m0} e^{i(\omega t - \beta_m z)}}_{\vec{E}} - \mu \epsilon \underbrace{\frac{\partial^2}{\partial t^2} \sum_m U_m E_{m0} e^{i(\omega t - \beta_m z)}}_{\vec{E}} = \mu \epsilon_0 \Delta n^2 \frac{\partial^2 \vec{E}}{\partial t^2} \quad (2.6)$$

$$\left\{ \sum_m E_{m0} e^{i(\omega t - \beta_m z)} \nabla_T^2 U_m + U_m \frac{\partial^2}{\partial z^2} [E_{m0} e^{i(\omega t - \beta_m z)}] \right\} - \mu \epsilon \left\{ \sum_m U_m E_{m0} \frac{\partial^2}{\partial t^2} e^{i(\omega t - \beta_m z)} \right\} \quad (2.7)$$

$$= \mu \epsilon_0 \Delta n^2 \frac{\partial^2 \vec{E}}{\partial t^2}$$

$$\sum_m E_{m0} e^{i(\omega t - \beta_m z)} \left[\underbrace{\nabla_T^2 U_m - \beta_m^2 U_m + \mu \epsilon \omega^2 U_m}_{=0 \rightarrow \text{Eq.2.5}} \right] + U_m \left[\frac{\partial^2 E_{m0}}{\partial z^2} - 2i\beta_m \frac{\partial E_{m0}}{\partial z} \right] e^{i(\omega t - \beta_m z)} \quad (2.8)$$

$$= \mu \epsilon_0 \Delta n^2 \frac{\partial^2 \vec{E}}{\partial t^2}$$

Notice the slow varying terms are neglected, i.e. the second derivative of E_{m0} with respect to z as compared to the first. Now the equation is reduced to a simple form

$$\sum_m -2i\beta_m \frac{\partial E_{m0}(z)}{\partial z} e^{i(\omega t - \beta_m z)} U_m(x, y) = \mu \epsilon_0 \Delta n^2 \frac{\partial^2 \vec{E}(\vec{r}, t)}{\partial t^2} \quad (2.9)$$

Now we multiply both sides of the equation by the U_s and integrate over the area of the waveguide.

$$\int \left(\sum_m -2i\beta_m \frac{\partial E_{m0}}{\partial z} e^{i(\omega t - \beta_m z)} U_m U_s \right) dA = \int \left(\mu \epsilon_0 \Delta n^2 \frac{\partial^2 \vec{E}}{\partial t^2} U_s \right) dA \quad (2.10)$$

One of the properties of the transverse eigenmode is that it is defined so each mode is orthogonal to each other and normalized such that

$$\int (U_m U_n) dA = \frac{2\omega\mu}{\beta_m} \delta_{mn} \quad (2.11)$$

By taking advantage of this property Eq.2.10 can be rewritten as

$$\begin{aligned} \sum_m -2i\beta_m \frac{\partial E_{m0}}{\partial z} e^{i(\omega t - \beta_m z)} \overbrace{\left(\frac{2\omega\mu}{\beta_m} \right) \delta_{ms}}^{\int (U_m U_n) dA} &= \int \left(\mu\epsilon_0 \Delta n^2 \frac{\partial^2 \bar{E}}{\partial t^2} U_s \right) dA \\ \frac{\partial E_{s0}^{bwd}}{\partial z} e^{i(\omega t + \beta_s z)} - \frac{\partial E_{s0}^{fwd}}{\partial z} e^{i(\omega t - \beta_s z)} &= -\frac{i\epsilon_0}{4\omega} \int \left(\Delta n^2 \frac{\partial^2 \bar{E}}{\partial t^2} U_s \right) dA \end{aligned} \quad (2.12)$$

This will give us a forward and a backward traveling wave as each value of m contains two terms involving U_m . For the electric field on the right side of Eq.2.12 we can plug in Eq.2.4 to yield

$$\begin{aligned} \frac{\partial E_{s0}^{bwd}}{\partial z} e^{i(\omega t + \beta_s z)} - \frac{\partial E_{s0}^{fwd}}{\partial z} e^{i(\omega t - \beta_s z)} &= -\frac{i\epsilon_0}{4\omega} \int \Delta n^2 \frac{\partial^2}{\partial t^2} \underbrace{\sum_m U_m E_{m0} e^{i(\omega t - \beta_m z)}}_{\bar{E}} U_s dA \\ \frac{\partial E_{s0}^{bwd}}{\partial z} e^{i(\omega t + \beta_s z)} - \frac{\partial E_{s0}^{fwd}}{\partial z} e^{i(\omega t - \beta_s z)} &= -\frac{i\epsilon_0}{4\omega} \frac{\partial^2}{\partial t^2} \sum_m \int \Delta n^2 U_m U_s E_{m0} e^{i(\omega t - \beta_m z)} dA \end{aligned} \quad (2.13)$$

In order for the m-components from the right side of Eq.2.13 to match the components on the left we must make $m=s$. This will translate to a term on the right to behave as a driving term for the term on the left. Both sides as described by waves must have the same frequency and phase. This will ensure that the two do not average out to zero over both time and propagation distance.

A closer look tells us that if the perturbation Δn^2 is a constant, then Eq.2.13 becomes two independent uncoupled equations describing the two modes traveling in opposite directions. This is not of any interest here. We are after the case that a term on

the right hand side of the equation going in one direction drives the term traveling in the opposite direction. We need a phase on the perturbation that will ensure this match.

$$\frac{\partial E_{s0}^{bwd}}{\partial z} e^{i(\omega t + \beta_s z)} = -\frac{i\epsilon_0}{4\omega} \frac{\partial^2}{\partial t^2} \int \Delta n^2 U_s^2 E_{s0} e^{i(\omega t - \beta_s z)} dA \quad (2.14)$$

Now let's consider a grating whose corrugation is described by a square wave as shown in Figure 2.1. Here the period of the perturbation is chosen so that $p\pi/\Lambda \approx \beta_s$. From the dimensions of the corrugation we will be able to find a formula that completely describes the perturbation in the index of refraction, namely $\Delta n^2(x,y,z)$.

This perturbation can be written as a product of the index of refraction in the z direction and its transverse direction. Furthermore the z -direction of the perturbation can be written as a Fourier series.

$$\begin{aligned} \Delta n^2(x, y, z) &= \Delta n^2(x, y) f(z) \\ \Delta n^2(x, y, z) &= \Delta n^2(x, y) \sum_q a_q e^{i\left(\frac{2q\pi}{\Lambda}\right)z} \end{aligned} \quad (2.15)$$

The index of refraction in the transverse direction, $\Delta n^2(x,y)$ is defined as an unperturbed waveguide material to be $1 - n_1^2$ within the material and 0 elsewhere. In the following section we will see how a thickness variation translates to a variation in the index of refraction. For now we can write the Fourier coefficients for the z dependent index of refraction from the amplitude of the perturbation in the index of refraction.

$$\begin{aligned} a_q &= \frac{1}{\Lambda} \left[\int_{-\frac{\Lambda}{2}}^0 (0) e^{-i\left(\frac{2q\pi}{\Lambda}\right)z} dz + \int_0^{\frac{\Lambda}{2}} (\Delta n_{amp}) e^{-i\left(\frac{2q\pi}{\Lambda}\right)z} dz \right] \\ a_q &= \frac{(\Delta n_{amp})}{\Lambda} \left(\frac{i\Lambda}{2q\pi} \right) [e^{-iq\pi} - 1] \Rightarrow a_q = \begin{cases} \frac{-i(\Delta n_{amp})}{q\pi} & q \text{ odd} \\ 0 & q \text{ even} \end{cases} \end{aligned} \quad (2.16)$$

Here we've defined Δn_{amp} to be the amplitude of the perturbation in the index of refraction. This Δn_{amp} shall be calculated for various examples in the following section.

Now that we have completely specified the index of refraction of this perturbation we can substitute it back into Eq.2.14. Recall that earlier we had set $m=s$. This was to ensure that the driven and source terms did not average out to zero over distance. The other requirement that we are after is that of a phase matching condition as explained earlier. The term on the left side of Eq.2.14 that describes the backward traveling wave, E_{s0}^{bwd} , has a phase associated equal to $+\beta_s$. A term exists on the right side with a phase of $2q\pi/\Lambda - \beta_s$ but the period of the corrugation was set such that this term is phase matched accordingly by making $p=q$. So we have a differential equation that describes how the forward traveling wave couples into the backward wave at the perturbation.

$$\begin{aligned} \frac{\partial E_{s0}^{bwd}}{\partial z} e^{i(\omega t + \beta_s z)} &= -\frac{i\varepsilon_0}{4\omega} \frac{\partial^2}{\partial t^2} \int \underbrace{\Delta n^2(x, y) \sum_q a_q e^{i\left(\frac{2q\pi}{\Lambda}\right)z}}_{\Delta n^2} U_s^2 E_{s0}^{fwd} e^{i(\omega t - \beta_s z)} dA \\ \frac{\partial E_{s0}^{bwd}}{\partial z} e^{i(\omega t + \beta_s z)} &= -\frac{i\varepsilon_0}{4\omega} \int \Delta n^2(x, y) a_p e^{i\left(\frac{2p\pi}{\Lambda}\right)z} U_s^2 E_{s0}^{fwd} \frac{\partial^2}{\partial t^2} e^{i(\omega t - \beta_s z)} dA \\ \frac{\partial E_{s0}^{bwd}}{\partial z} &= \frac{i\varepsilon_0 \omega}{4} E_{s0}^{fwd} a_p e^{i\left(\frac{2p\pi}{\Lambda} - 2\beta_s\right)z} \int \Delta n^2(x, y) U_s^2 dA \end{aligned} \quad (2.17)$$

The detuning frequency is defined as $\beta_d = p\pi/\Lambda - \beta_s$. The importance behind this tuning parameter is essential to making the two waves coupled. The period of the corrugation shall be selected to as to make this detuning as close to zero. Note that as it goes to zero we have that $\Lambda = p\pi/\beta_s$. By defining yet another parameter the guide wavelength of the s-mode as $\lambda = 2\pi/\beta_s$, then we see that the period of the grating must be tuned to the wavelength as the Bragg condition defined by

$$\Lambda = \frac{p\pi}{\beta_s} = \frac{p\pi}{2n\pi/\lambda} = \frac{p\lambda}{2n} \quad (2.18)$$

The value as defined by p will determine the order of the gratings. Another parameter that groups the integral and the rest of the constants as

$$\kappa = \frac{i\varepsilon_0\omega a_p}{4} \int \Delta n^2(x, y) U_s^2 dA \quad (2.19)$$

As defined this parameter will be dependent on the geometry of the gratings. The refractive index in the transverse direction will determine this value. Note that this parameter is linearly dependent on the Fourier coefficient as defined before. The order of the gratings will thus affect this parameter and thus the strength of the gratings. With this definition the coupled equations can be written as

$$\begin{aligned} \frac{\partial E_{s0}^{bwd}(z)}{\partial z} &= \kappa E_{s0}^{fwd}(z) e^{i2\beta_d z} \\ \frac{\partial E_{s0}^{fwd}(z)}{\partial z} &= \kappa^* E_{s0}^{bwd}(z) e^{-i2\beta_d z} \end{aligned} \quad (2.20)$$

2.1.3. Effective Index Method for DBR laser

Bragg Gratings can be implemented in a waveguide material to make DBR and DFB lasers. Here we study the behavior of a DBR in a particular example

The example to be studied here consists of a three layered waveguide material depicted in Figure 2.2. The substrate on the bottom is InP whose index of refraction is 3.14 and designed with a thickness of $3\mu\text{m}$ and a width of $9\mu\text{m}$. The material on top is also InP and here there is a $3\mu\text{m}$ wide ridge with a thickness of $1.5\mu\text{m}$.

The middle layer is the active region, made up of GaInAs whose index of refraction is 3.55. It is in this middle region where a corrugation of the material will

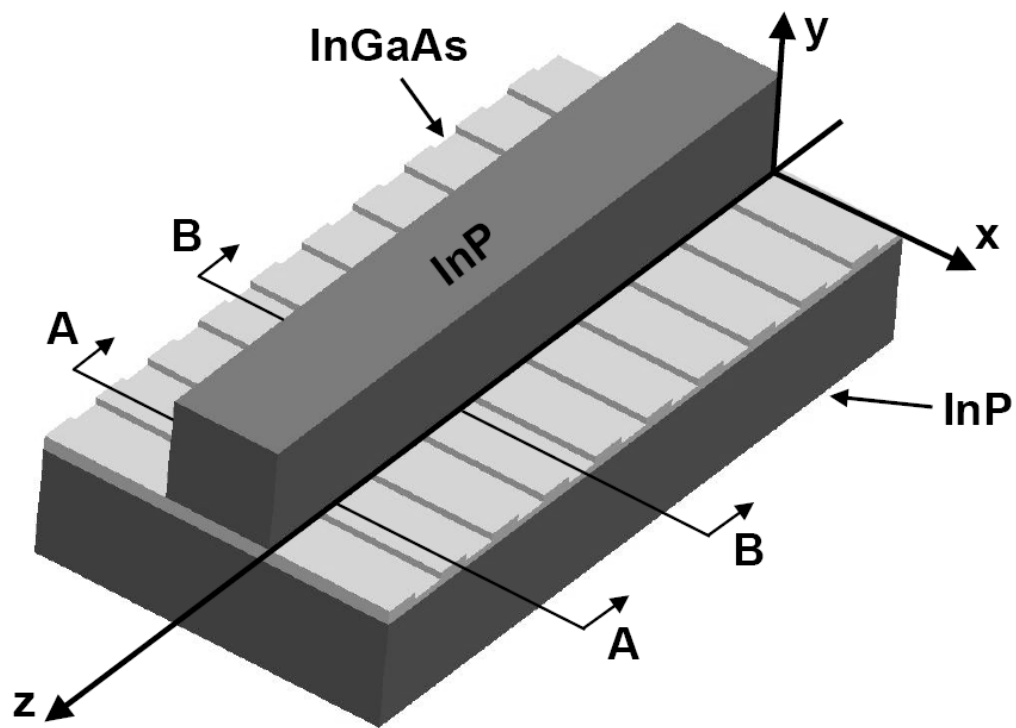


Figure 2.2: Fictional DBR laser to help understand behavior of Bragg Gratings. Effective index method looks at the two cross sections A-A and B-B.

define the gratings. The entire thickness of the material is 200nm and it is as wide as the bottom, $9\mu\text{m}$. The gratings have a depth of 100nm, half of the thickness of the active region. The periodicity of the gratings shall be set as Λ .

The design of the device to be studied here has been specified in order to simplify the analysis of the problem. Although only this particular case is being studied we will still be able to get a feel for how the depth of the gratings affects the index of refraction.

First we begin our analysis by using the effective index method to calculate how the index of refraction changes along the gratings. That is we shall calculate the effective index of refraction for the scheme defined by both cross sections A-A and B-B. The difference between the two is determined by the amplitude of the corrugation made. As mentioned the gratings is simply a corrugation of the active region. It is simply a variation in height that oscillates in this case between two values. Other gratings can be made up of sinusoidal waves or even triangular shapes. Here we will study the square wave case shown.

The two height changes the active region oscillates between, translates to a change in the effective index of refraction. The two heights are described by cross section A-A and B-B. We can calculate the effective index of refraction for each case in order to understand how this phenomenon.

First we look at section AA depicted in Figure 2.3. We can break this down into three different regions as shown. A closer look at cross sections tells us the problem is symmetric about the y-axis and so we only need to look at two different regions, namely I and II.

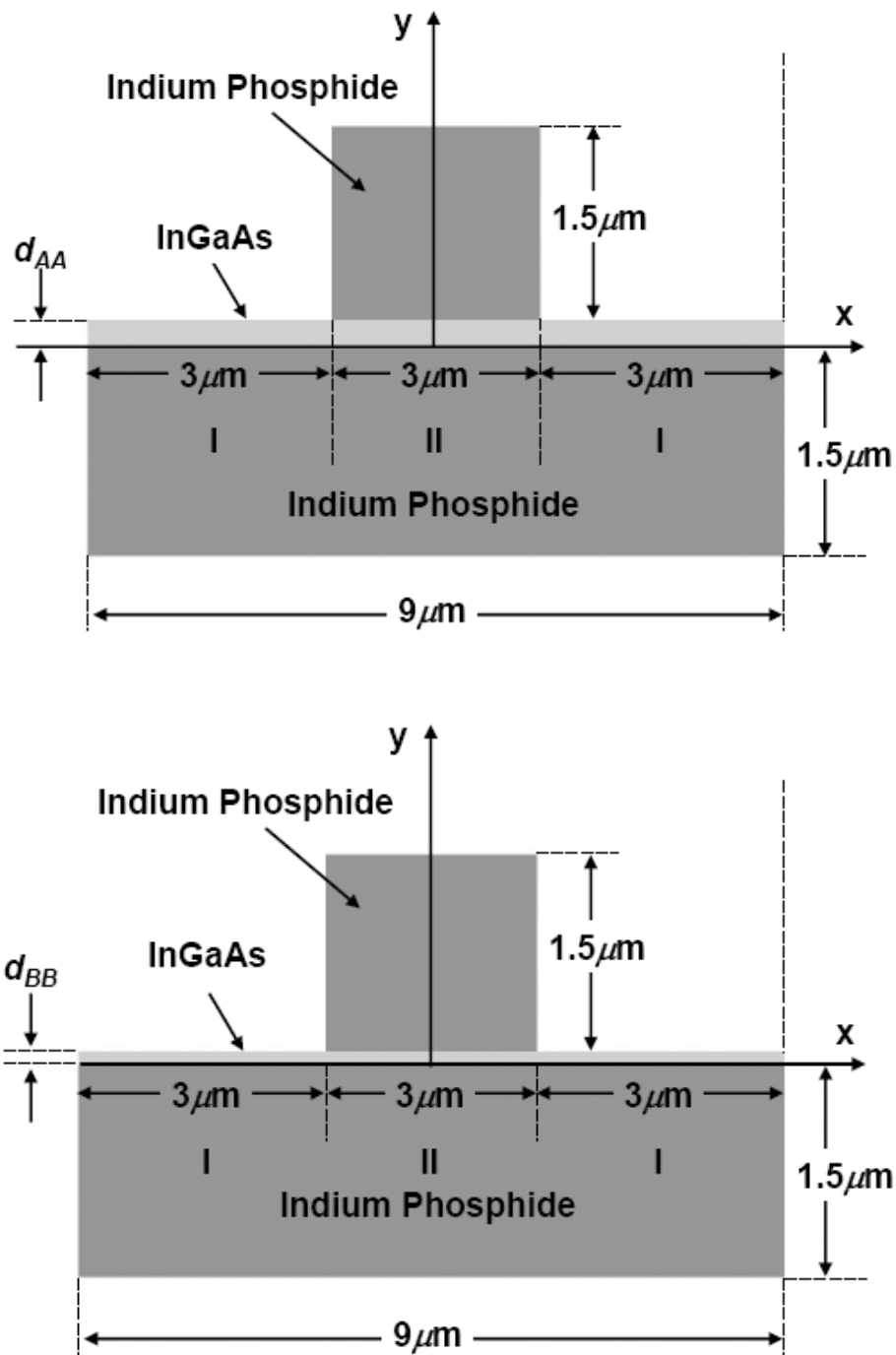


Figure 2.3: Cross sections A-A and B-B respectively. The difference between the two is the variation in thickness of the active region InGaAs. d oscillates between 100nm and 200nm that defines the gratings.

Section I is essentially an asymmetric slab composed of three layers. We can further break this section down along the y-direction into another three subgroups and look at the electric field in the three different subsections. These subsections will be defined by numbers 1, 2, and 3.

Please note that we are breaking the entire cross section A-A into three regions, where two are identical so we have section I and II. Here we are looking at the electric field in section I. In order to realize this we are breaking this section along the y-direction into *another* three subsections, 1, 2, and 3.

We begin our analysis with the wave equation, as derived from Maxwell's equation that describes the electric field as

$$\nabla^2 \vec{E} - \mu\epsilon \frac{\partial^2}{\partial t^2} \vec{E} = 0 \quad (2.21)$$

Knowing that the electric field is a time-harmonic field with frequency ω traveling in the z-direction with phase β , this can be rewritten to look like

$$\nabla_T^2 \vec{E} + (k_0^2 n_i^2 - \beta^2) \vec{E} = 0 \quad (2.22)$$

where $k_0^2 = \omega^2 \mu_0 \epsilon_0 = (2\pi/\lambda)^2$ and n_i is the index of refraction of the medium. The phase defined as β can be rewritten in terms of the phase velocity as $\beta = \omega/v_p$ which by rewriting it allows us to introduce this effective index defined as

$$\beta = \omega/v_p = \omega n_{eff} / c = k_0 n_{eff} \quad (2.23)$$

Because of the way the layers are defined we have a TM mode. That is the fields both electric and magnetic are all zero except for E_y , E_z , and H_x . A solution to Eq.2.22 for the electric field can be written for each layer as it depends on the geometry of that

region. This is a well known problem that has been solved in many literatures [11]. So we simply write the solution for E_z as

$$\begin{aligned} E_{z1} &= Ae^{-\gamma_1(y-d)} & d \leq y & \quad (\text{layer1}) \\ E_{z2} &= B \cos(k_2 y) + C \sin(k_2 y) & 0 \leq y \leq d & \quad (\text{layer2}) \\ E_{z3} &= De^{\gamma_3 y} & y \leq 0 & \quad (\text{layer3}) \end{aligned} \quad (2.24)$$

In order to get values for each parameter that describes the electric field in the different regions we look at the boundary conditions in each case. Because of the polarization mentioned we have to look at the continuity of the magnetic field across the border. From Maxwell's equation we know that

$$\nabla \times \vec{H} = \frac{\partial \vec{D}}{\partial t} = \varepsilon \frac{\partial \vec{E}}{\partial t} \quad (2.25)$$

Since only H_x is non-zero and the electric field is a time harmonic field as defined above this reduces to

$$\vec{z} \left(-\frac{\partial H_x}{\partial y} \right) = \varepsilon (i\omega) \vec{z} E_z \quad (2.26)$$

Now we can use some calculus and integrate the electric field to get fields for the magnetic in the x-direction.

$$\begin{aligned} H_{x1} &= \frac{i\varepsilon_1 \omega}{\gamma_1} Ae^{-\gamma_1(y-d)} & d \leq y & \quad (\text{layer1}) \\ H_{x2} &= \frac{i\varepsilon_2 \omega}{k_2} [C \cos(k_2 y) - B \sin(k_2 y)] & 0 \leq y \leq d & \quad (\text{layer2}) \\ H_{x3} &= -\frac{i\varepsilon_3 \omega}{\gamma_3} De^{\gamma_3 y} & y \leq 0 & \quad (\text{layer3}) \end{aligned} \quad (2.27)$$

Now we are ready to look at the boundary conditions. From Maxwell's equations we know that both $\nabla \cdot B = 0$ and $\nabla \cdot D = 0$. From these two equations we can write that

the tangential electric and magnetic fields are both continuous at the boundaries. At $y=0$ we have

$$-\frac{i\varepsilon_3\omega}{\gamma_3}D = \frac{i\varepsilon_3\omega}{k_2}C \quad \Rightarrow \quad B = D = -\frac{\gamma_3\varepsilon_2}{k_2\varepsilon_3}C \quad (2.28)$$

from continuity of both electric and magnetic. At $y=d$ we have that

$$\begin{aligned} A &= B \cos k_2d + C \sin k_2d \\ \frac{i\varepsilon_1\omega}{\gamma_1}A &= \frac{i\varepsilon_2\omega}{k_2} \{C \cos k_2d - B \sin k_2d\} \end{aligned} \quad (2.29)$$

With some algebra we can get a transcendental equation

$$\tan k_2d = \frac{\left(\frac{\gamma_1}{k_2}\right)\left(\frac{\varepsilon_2}{\varepsilon_1}\right) + \left(\frac{\gamma_3}{k_2}\right)\left(\frac{\varepsilon_2}{\varepsilon_3}\right)}{1 - \left(\frac{\gamma_1\gamma_3}{k_2^2}\right)\left(\frac{\varepsilon_2^2}{\varepsilon_1\varepsilon_3}\right)} \quad (2.30)$$

By substituting in the electric field of the three different subsections into the wave equation with the appropriate indices of refraction we can get a relation for the different parameters used to describe the field.

$$\begin{aligned} \gamma_1^2 &= \beta^2 - k_0^2n_1^2 \\ k_2^2 &= k_0^2n_2^2 - \beta^2 \\ \gamma_3^2 &= \beta^2 - k_0^2n_2^2 \end{aligned} \quad (2.31)$$

Also the different dielectric coefficients are defined as $\varepsilon_i = \varepsilon_0n_i^2$. By plugging these back into Eq.2.30 we get

$$\tan k_2d = \frac{\left(\frac{\gamma_1}{k_2}\right)\left(\frac{n_2^2}{n_1^2}\right) + \left(\frac{\gamma_3}{k_2}\right)\left(\frac{n_2^2}{n_3^2}\right)}{1 - \left(\frac{\gamma_1\gamma_3}{k_2^2}\right)\left(\frac{n_2^4}{n_1^2n_3^2}\right)} \quad (2.32)$$

Recall that earlier we had defined the phase as $\beta = k_0 n_{eff}$. Now we can proceed to calculating the effective index of refraction for this asymmetric section I.

The first layer is just air with an index of refraction equal to $n_1=1.0$. The middle layer, the active region has $d=200\text{nm}$ for cross section A-A and has an index of refraction of 3.55. Finally layer 3 is made of InP with an index of refraction $n_3=3.14$.

By varying the effective index of refraction, n_{eff} , we can find when the right side of Eq.2.32 is equal to the left. Here the value for section I is calculated using MATLAB to be $n_1=3.168$. Matlab code is available in Appendix D.

This is the index of refraction for the left section of cross section A-A which is identical to the section on the right side. So we have found two of the three indices of refraction needed to fully describe section A-A. We continue by looking at the middle section defined along the x-axis, namely section II.

This section is another three layer section with the difference that it is symmetric about the x-axis. We have InP on the bottom layer, InGaAs in the middle layer and finally another layer of InP. So here $n_1=n_3$.

Because of the polarization and geometry of the three layered structure we again have TM modes. Again the electric and magnetic fields will be continuous across the boundaries.

A similar analysis to the one used for the asymmetric case allows to calculate the transcendental equation for the symmetric case. This equation will in turn allow us to calculate the effective index of refraction, n_{II} . Because of the symmetry the coefficients that describe the fields for the two outermost layers are equal, $\gamma_1 = \gamma_3$.

$$\tan k_2 d = \left(\frac{n_2^2}{n_1^2} \right) \left(\frac{\gamma_1}{k_2} \right) \quad (2.33)$$

Again we can use MATLAB to solve this transcendental equation. Here the index of refraction is equivalent to $n_{II}=3.369$.

We have found all indices of refraction for the three sections in A-A. Now we are left with an equivalent three layer slab positioned along the x-axis. Section II with its index of refraction n_{II} sandwiched in between the two identical section I.

Now the electric field is oriented in the same way and so we have a TE mode. That is the electric field pointing in either the y or z-direction as mentioned before. Now we can look at the continuity of the tangential electric and magnetic fields across the boundaries. The transcendental equation derived.

$$\tan k_2 d = \left(\frac{\gamma_1}{k_2} \right) \quad (2.34)$$

Here the effective index is varied again and its value is found to be $n_{AA}=3.367$. We have completely determined all effective index calculations for cross section A-A. A similar analysis is performed for cross section B-B and a value of 3.235 is obtained for the effective index. Results are summarized for both cross sections in Table 2.1.

Table 2.1a

Index of refraction xsection AA		Sections (x-axis)		
		I	II	I
Subsection (y-axis)	1	1	3.17	1
	2	3.55	3.55	3.55
	3	3.17	3.17	3.17
effective index, n_{eff}		3.168	3.369	3.168

Table 2.1b

Index of refraction xsection BB		Sections (x-axis)		
		I	II	I
Subsection (y-axis)	1	1	3.17	1
	2	3.55	3.55	3.55
	3	3.17	3.17	3.17
effective index, n_{eff}		3.157	3.254	3.157

Table 2.1c

n_{AA}	3.367
n_{BB}	3.252

Table 2.1: Results for the effective index method summarized. a)cross section A-A, b)cross section B-B and c)final values

With the values of the effective index for each section we can find values for the parameters that describe the electric field in each subsection. Here we look only at cross section AA to understand better how the field decays in each different region. A similar analysis can be realized for BB not depicted here.

Figure2.4a shows the field in section I. As expected the field decays much faster in the air then it does in the substrate. In Figure2.4b however the field is symmetric about $y=0$ because of the geometry of the slab. The solution to this symmetric case resembles that of a solution to the Schrödinger's equation.

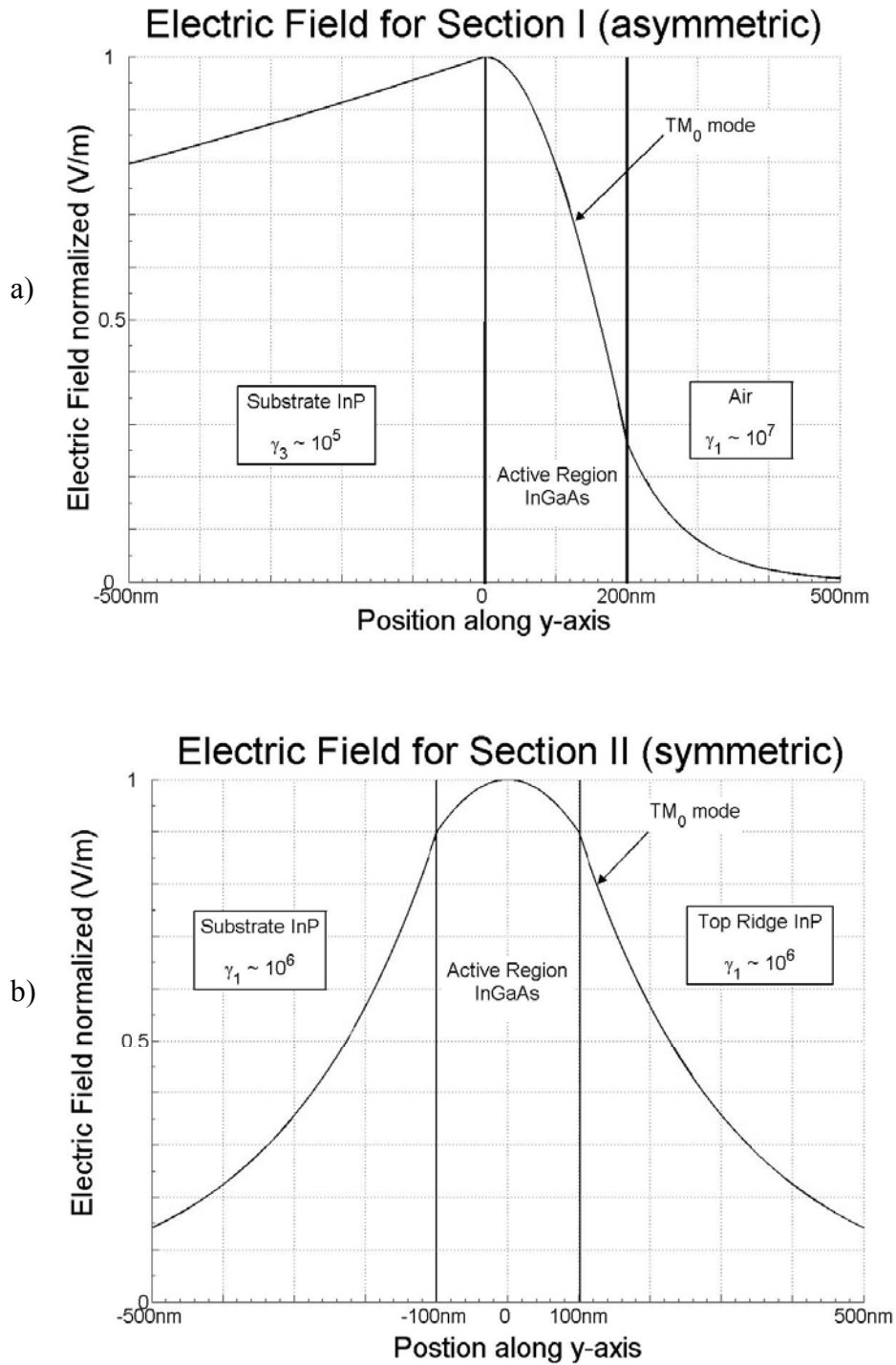


Figure 2.4: The Electric field in the two different sections I and II. Section I (a) is an asymmetric slab while section II (b) is symmetric.

Now that we have the two different effective indices of refraction for cross section AA and BB we can see how this translates to the gratings. As derived in the previous section the coefficient that determines the strength of the gratings is

$$\kappa = \frac{i\varepsilon_0\omega a_p}{4} \int \Delta n^2(x, y) U_s^2 dA \quad (2.35)$$

which can be rewritten from the Fourier coefficient defined in Eq.2.16

$$\kappa = + \frac{\varepsilon_0\omega\Delta n_{amp}}{4p\pi} \int \Delta n^2(x, y) U_s^2 dA \quad (2.36)$$

Now we can look at first order gratings since they are the strongest. Substituting in all the values and integrating across the waveguide we get $\kappa = 263.5\text{m}^{-1}$ for $d_{AA}=200\text{nm}$ and $d_{BB}=100\text{nm}$. With this value for κ we will be able to see what length of gratings is needed for desired maximum reflectivity.

A more thorough analysis will give us a better understanding of how the index of refraction contrast Δn_{amp} will depend on the difference in thickness between the two cross sections AA and BB. Figure 2.5 shows various curves for different thickness of the active region. Because of the method used to determine the different effective indices of refraction we cannot simply write an equation for Δn_{amp} that will depend on the thickness difference, $d_{AA} - d_{BB}$.

There is however a few things we can say about the curves presented. The first observation which is quite general is that as the thickness difference increases, Δn_{amp} increases as well. Also as the thickness of cross section AA increases, a higher thickness difference is needed to achieve the same Δn_{amp} , though a higher Δn_{amp} can be obtained for a bigger thickness difference.

Index of Refraction Contrast

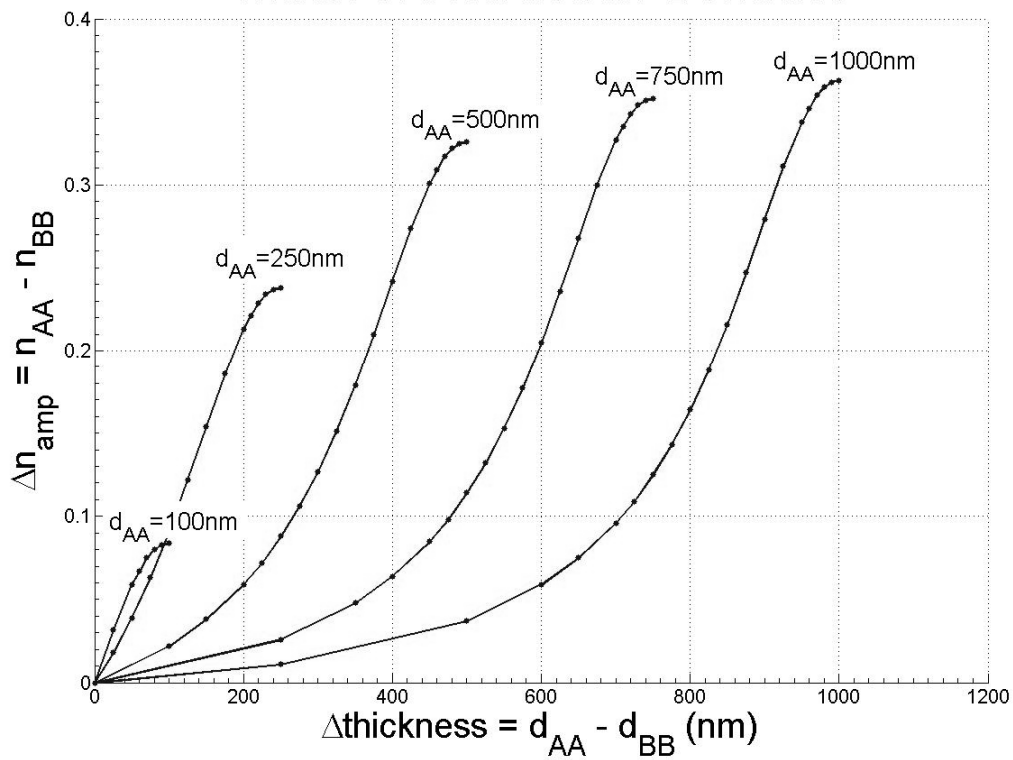


Figure 2.5: Qualitative look at how the thickness variation will change the index of refraction contrast. A index contrast of $\Delta n_{amp} = 0.115$ will translate to $\kappa = 263.5\text{m}^{-1}$ as was calculated.

The slopes for the curves of thinner thickness are higher in the lower region. One could infer that in the lower region of the thickness difference, a variation in the thickness will translate to a higher index contrast. Take the example used to calculate κ in this section, $d_{AA}=200\text{nm}$ and $d_{BB}=100\text{nm}$ and another with thicknesses of $d_{AA}=1000\text{nm}$ and $d_{BB}=900\text{nm}$. The thickness difference is the same 100nm but the first will translate to a higher contrast in index of refraction Δn_{amp} than the latter.

2.1.4. Finite Length Gratings

Let's suppose we have a wave traveling in the forward direction in the beginning of the gratings, $z=0$. As mentioned this will cause part of the wave to be reflected and another to be transmitted. The reflectivity can be defined as magnitude squared of the ratio of the backward traveling wave to the forward traveling wave at $z=0$. This has been calculated in [12] with detuning at zero to be

$$R_{Max} = \left| \frac{E_{s0}^{bwd}(0)}{E_{s0}^{fwd}(0)} \right|^2 = \left| \tanh[\kappa L_g] \right|^2 \quad (2.37)$$

With the value as calculated in the previous section for κ , we can plot to see how the reflectivity varies for different lengths of the gratings. Figure 2.6 shows gratings of length 10mm will produce a reflectivity of better than 0.95

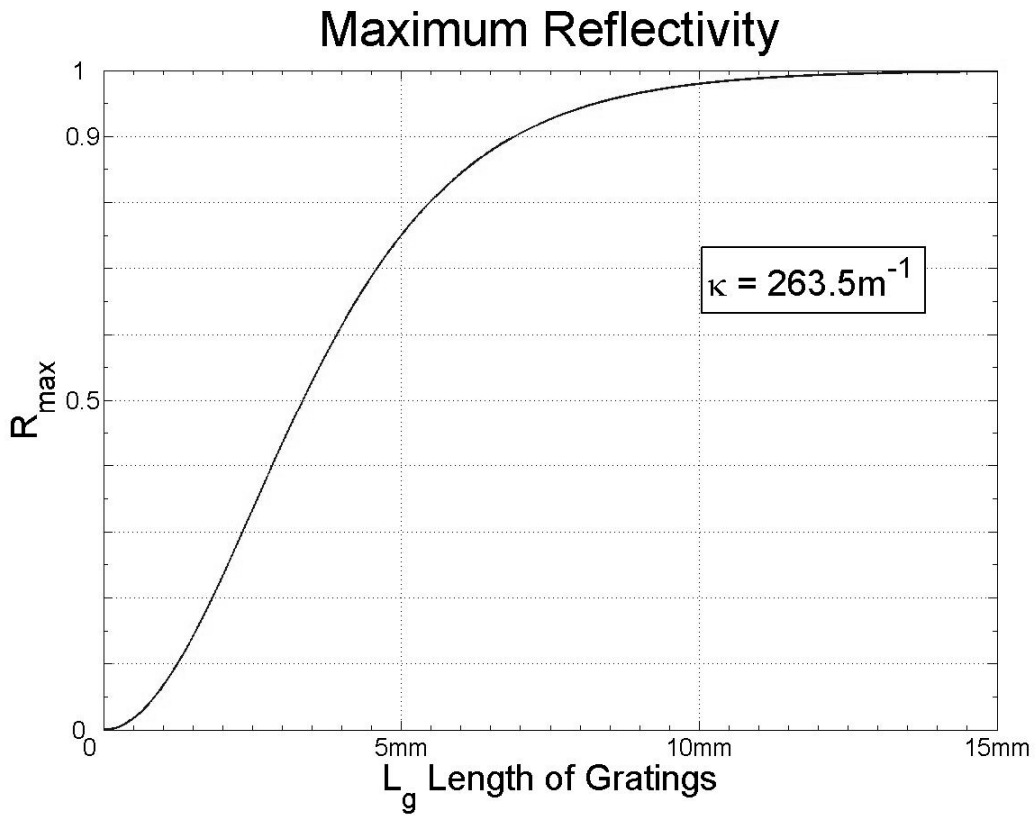


Figure 2.6: Maximum Reflectivity for Bragg Gratings. Reflectivity increases rapidly as the length increases.

2.2. Standing Wave

In order to fabricate Bragg Gratings a series of steps are followed discussed with detail in Chapter 4. One of the steps is to expose positive resist with an interference pattern created by two waves at an angle of incidence, θ . In this section we discuss how this interference is created and how its period varies with the angle of incidence.

2.2.1. Interference of Light

When two plane waves interfere with each other as shown in Figure 2.4, a standing wave is produced. The periodicity of the standing wave created on the substrate is calculated from the angle of the two waves and their wave vector, \vec{k} . Here a different set of arbitrary coordinates is used to calculate the period of the interference pattern.

The problem to be solved in this section is realized by looking at the wave vectors of the two interfering waves. Before we proceed with this calculation however, the problem considered here takes into account a few assumptions. The first is that the two waves have the same magnitude, E_0 . It is shown later however that a difference in magnitudes will not affect the interference pattern considerably. Second we assume that the two waves have the same angle of incidence, θ . Finally their wave vectors, \vec{k}_1 and \vec{k}_2 , have the same magnitudes but their directions differ in the x-component.

Now we can begin by describing each of the two waves with their electric field pointing in the y-direction as shown.

$$\begin{aligned}\vec{E}_1 &= \vec{y}E_0e^{i(\vec{k}_1 \cdot \vec{x} - \omega t)} \\ \vec{E}_2 &= \vec{y}E_0e^{i(\vec{k}_2 \cdot \vec{x} - \omega t)}\end{aligned}\tag{2.23}$$

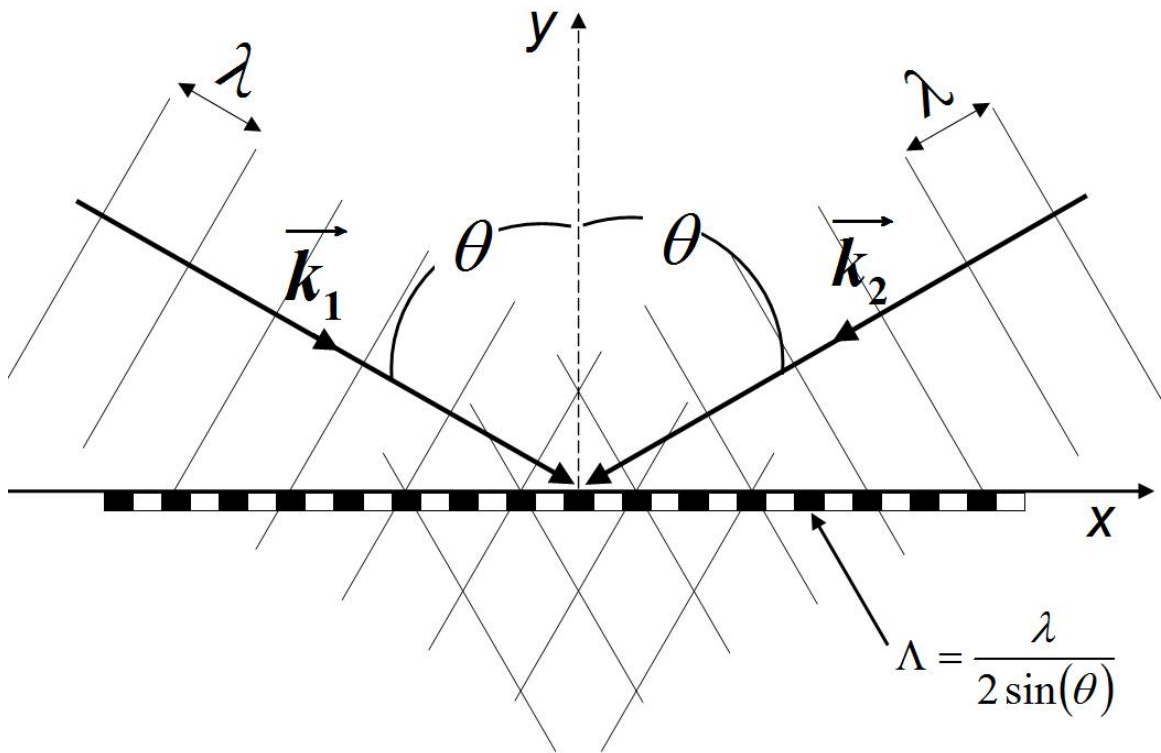


Figure 2.4: When two plane waves interfere at angle 2θ , a standing wave is created whose periodicity depends on half of that angle

From these two waves an expression for the total electric field can be calculated

$$\vec{E}_{Total} = \vec{y}E_0 e^{-i\omega t} \left[e^{i\vec{k}_1 \cdot \vec{x}} + e^{i\vec{k}_2 \cdot \vec{x}} \right] \quad (2.24)$$

then an expression for the intensity of the total electric field as the square of the magnitude of the amplitude

$$\begin{aligned} I_{Total} &= \left| \vec{E}_{Total} \right|^2 = \left\{ \vec{E}_{Total} \right\} \cdot \left\{ \vec{E}_{Total} \right\}^* \\ I_{Total} &= \left\{ \vec{y}E_0 e^{-i\omega t} \left[e^{i\vec{k}_1 \cdot \vec{x}} + e^{i\vec{k}_2 \cdot \vec{x}} \right] \right\} \cdot \left\{ \vec{y}E_0 e^{i\omega t} \left[e^{-i\vec{k}_1 \cdot \vec{x}} + e^{-i\vec{k}_2 \cdot \vec{x}} \right] \right\} \\ I_{Total} &= E_0^2 \left[2 + e^{i(\vec{k}_1 \cdot \vec{x} - \vec{k}_2 \cdot \vec{x})} + e^{-i(\vec{k}_1 \cdot \vec{x} - \vec{k}_2 \cdot \vec{x})} \right] \\ I_{Total} &= E_0^2 \left[2 + 2 \cos(\vec{k}_1 \cdot \vec{x} - \vec{k}_2 \cdot \vec{x}) \right] \\ I_{Total} &= 4E_0^2 \cos^2 \left(\frac{\vec{k}_1 \cdot \vec{x} - \vec{k}_2 \cdot \vec{x}}{2} \right) \end{aligned} \quad (2.25)$$

Now we are almost ready to calculate the period of the standing wave created by these two plane waves. Before proceeding let's look at what the wave vectors represent. That is by decomposing the two dot products inside the sinusoid, we can figure out what the period is.

$$\begin{aligned} \vec{k}_1 \cdot \vec{x} - \vec{k}_2 \cdot \vec{x} &= (-k_x x + k_y y + k_z z) - (k_x x + k_y y + k_z z) \\ \vec{k}_1 \cdot \vec{x} - \vec{k}_2 \cdot \vec{x} &= -2k_x x \end{aligned} \quad (2.26)$$

By plugging in, the intensity becomes,

$$\begin{aligned} I_{Total} &= 4E_0^2 \cos^2 \left(\frac{\vec{k}_1 \cdot \vec{x} - \vec{k}_2 \cdot \vec{x}}{2} \right) = 4E_0^2 \cos^2 \left(\frac{-2k_x x}{2} \right) \\ I_{Total} &= 4E_0^2 \cos^2(-k_x x) = 4E_0^2 \cos^2(k_x x) \end{aligned} \quad (2.27)$$

The period of the sinusoid that describes the intensity seems to be negative. This however is arbitrary, since the function is even. Also we are after the period, the spacing

between the maxima, a negative period just refers to which direction in the x-direction it is pointing and this definition of the x-axis is completely arbitrary.

It is well known that the period of the square of a cosine can be determined by

$$\frac{\pi}{\Lambda} = k_x \quad (2.28)$$

The x-component of the wave vector is calculated from trigonometry as

$$k_x = k \sin \theta = \left(\frac{2\pi}{\lambda} \right) \sin \theta \quad (2.29)$$

Plugging this into Eq.2.28 gives the period of the interference pattern intensity

$$\Lambda = \frac{\pi}{k_x} = \frac{\pi}{\left(\frac{2\pi}{\lambda} \sin \theta \right)} = \frac{\lambda}{2 \sin \theta} \quad (2.30)$$

2.2.2. Unwanted Standing Wave

The interfering plane waves analyzed in the previous section create a standing wave not only in the x-direction but also one in the z-direction. Having a standing wave in the z-direction changes the exposing pattern. One way to avoid this issue is to deposit an antireflective coating that eliminates this unwanted standing wave. Although this method works quite well, it adds another complex step to the already challenging task at hand.

Let's begin this calculation by assuming that the standing wave in the z-direction is sinusoid. We can define the variation of the amplitude in this direction to be dependent on $\sin(kz)$. An unwanted wave will have half of the period span the thickness of the resist, d . Thus we have that

$$\sin(k * 2d) = \sin\left(\left\{\frac{2n_{res.}\pi}{\lambda}\right\} 2d\right) = 0 \quad (2.31)$$

$$\frac{4n_{res.}\pi d}{\lambda} = 2\pi \quad \Rightarrow \quad d = \frac{\lambda}{2n_{res.}} = 95.6nm$$

By making the thickness of the resist $\frac{1}{4}$ of the period or half of this thickness, 50nm, the unwanted standing wave will not be able to have any effect when exposing the sample.

Chapter 3: Experimental Setup / Design

This chapter of the thesis deals mainly with the setup used to expose the resist on top of the semiconductor. There are different methods that can be used to expose a sample under the interference of two sources such as the Mach-Zehnder Interferometer among others. Despite the repeatable exposure of the highest quality grating images, the Mach-Zehnder Interferometer requires precise alignment, a dedicated set of expensive optics and other complications. A simpler configuration however exists called the Lloyd's-Mirror Interferometer. Although much simpler than other setups, different decisions need to be made for it to work appropriately.

3.1. Lloyd's Mirror Setup

An overview of the implementation of the Lloyd's Mirror Interferometer is presented in Figure 3.1. The beam of the laser passes through various elements before getting to the sample. First a shutter is used to control the time of exposure. After the shutter, a turning mirror, two iris diaphragms, and another turning mirror are used to redirect the beam. The beam then passes through a spatial filter that both expands it and cleans it of any unwanted higher frequencies. The spatial filter used consists of a UV objective lens (EFL=13mm, effective focal length) and a 15 μ m diameter pinhole. Reasons for the EFL of the objective and pinhole size are explained later. Finally the beam reaches the Lloyd's Mirror where the interference is created.

The Lloyd's Mirror Interferometer consists of both a sample holder and an UV coated aluminum mirror placed orthogonal to each other. The expanded beam is directed at the center of where these two intersect. On half of the beam is directly incident on the

Experiment Setup

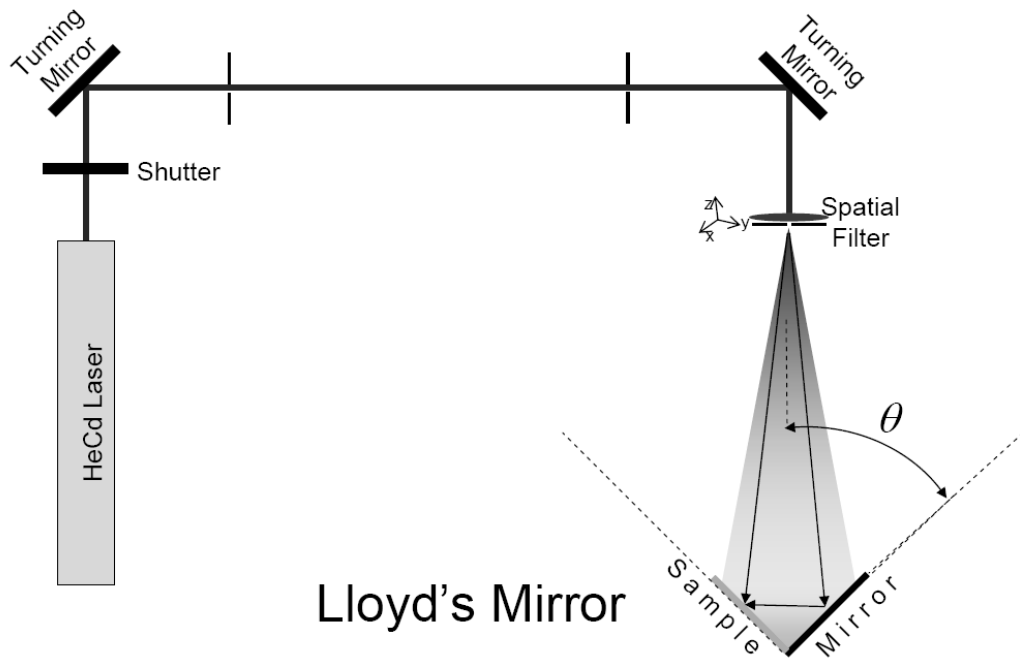


Figure 3.1: An overview of the setup used to create the interference pattern on the sample. A spatial filter is used to expand the beam (HeCd, $\lambda=325\text{nm}$) before it reaches the Lloyd's Mirror. The rotation stage used to hold the Lloyd's Mirror and sample allow for a change in the period of the grating made.

sample while the other half reflects off the mirror then onto the sample. The two half beams create an interference pattern on the sample, which creates the grating pattern. The Interferometer is placed on a rotation stage that allows for tuning of the Bragg Grating period, Λ . As shown the grating period is directly dependent on the angle of the incident beam

$$\Lambda = \frac{\lambda}{2\sin(\theta)} \quad (3.1)$$

where $\lambda=325\text{nm}$ is the wavelength of the HeCd laser, and θ is the angle of the incident beam.

3.2. Propagating a Gaussian

As mentioned in the setup the laser passes through various elements before getting to the Lloyd's Mirror. In a nutshell the laser slowly expands up to the lens, gets focused to its beam waist, and finally gets expanded again at a faster rate up to the Lloyd's Mirror. To better follow the calculations of the setup parameters described in this section, Figure 3.2 illustrates the experimental setup in this nutshell

All parameters calculated here are essential to ensuring the sample gets exposed properly. However there is an order of importance in which these values were determined. First, to ensure small variation of the electric field amplitude incident the sample, the focal length and location of the lens were determined relative to the Lloyd's Mirror. Second, a pinhole is placed at the beam waist after the lens to create a spatial filter that cleans the beam of any higher unwanted frequencies. All other parameters are still essential to the setup working properly but are of secondary importance.

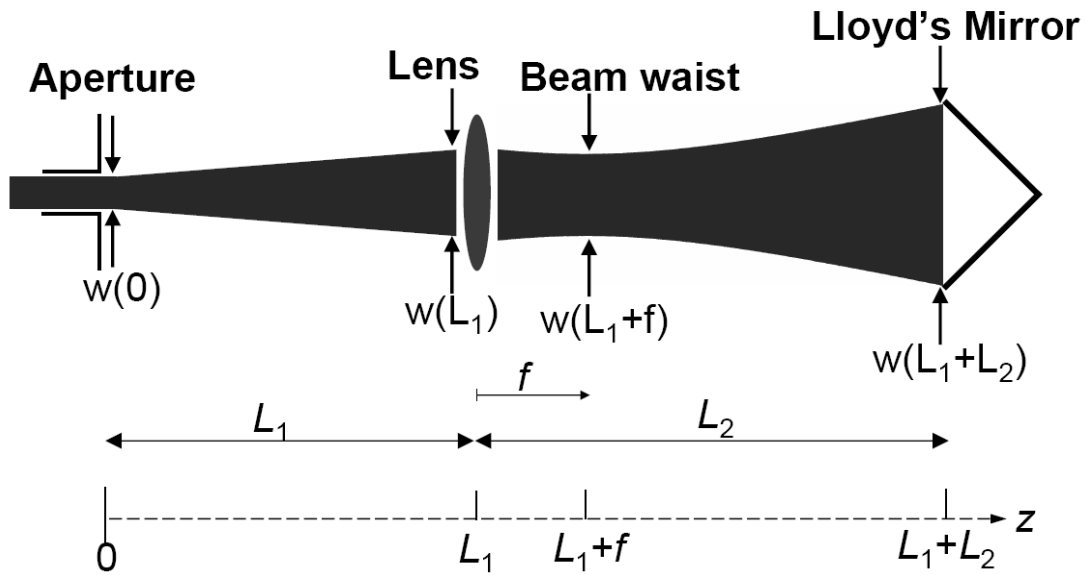


Figure 3.2: Here the setup has been simplified and dimensions exaggerated. This will aid the reader to follow the calculations under Propagating a Gaussian

Despite this order of importance, the calculations realized in this section follow the order in which the beam travels. First we begin by looking at the laser cavity to start with some initial values for the diameter of the beam. Then we proceed with an analysis for the propagation of the laser as it comes out of the aperture and up to the lens. Then using the result found in the first two parts the lens's parameters can be calculated. In the subsequent section an analysis of the laser as it travels from the lens up to the Lloyd's Mirror is performed to determine how the amplitude of the electric field behaves incident the sample. Finally the pinhole size needed is determined from these results to ensure a clean beam of any higher frequencies or scattering from particles.

3.2.1. Laser Cavity

In this first section we go through an extensive analysis of the cavity that allows us to determine specific values needed. The setup of the cavity will let us determine both the diameter at the beam waist and a value for the complex radius of curvature at the curved mirror.

The laser used in this experiment is a UV Helium Cadmium laser at $\lambda=325\text{nm}$ from Kimmon Electronics (Model IK3151R-E). As specified by the manufacturer the laser cavity is composed of two mirrors, a spherical with radius $R_1=5\text{m}$ and a flat ($R_2=\infty$), with a spacing between them of $L=91\text{cm}$.

From the dimensions of the laser cavity it is obvious that the beam waist will be located at the flat mirror. At the other mirror the radius of the beam will be the radius of mirror 1 at a distance of $L=91\text{cm}$ away. By using the properties of half-symmetric

resonators, all the necessary parameters can be calculated. We begin with the g parameter as defined in [13]

$$g = 1 - \frac{L}{R_1} = 1 - \frac{0.91m}{5m} = 0.818 \quad (3.2)$$

From this g parameter the waist at the different locations can be calculated as

$$\begin{aligned} w_1^2 &= \frac{L\lambda}{\pi} \sqrt{\frac{1}{g(1-g)}} \Rightarrow w_1 = 0.988mm \\ w_0^2 = w_2^2 &= \frac{L\lambda}{\pi} \sqrt{\frac{g}{1-g}} \Rightarrow w_0 = 0.894mm \end{aligned} \quad (3.3)$$

This means that at the spherical mirror, the beam has a diameter of 0.988mm and radius of curvature equal to that of the mirror's radius ($R_1=5m$). Meanwhile at the flat mirror, the beam waist has a diameter of 0.894mm and a radius of ∞ .

We have found all the values we need in order to proceed with calculating the desired parameters from the propagation law. However there is a subtle yet important point to make about the cavity. The two mirrors are inside this “black box” which means that either the flat or the spherical can be located near the aperture where the laser is emitted. That is, the two mirrors that make up the resonator can be oriented in one of two ways. Intuitively the flat mirror should be placed nearest the aperture in order to minimize the beam diameter. In order to be sure, a measurement of the beam diameter 10cm from the aperture is found to be 0.89mm in the data sheet of the laser. Since this measured value is much closer to that of the beam waist $w_0 = 0.894mm$, one can conclude the flat mirror is located closer to the aperture and the spherical mirror is located on the other side of the cavity.

Another important point to make is that the longest side of the black box (102.0cm) completely spans the distance between the two mirrors (91cm). Most likely this was designed to ensure some space between the walls of the black box and the two mirrors. This entails that we can only determine the location of the two mirrors within a range of $102.0\text{cm} - 91.0\text{cm} = 11.0\text{cm}$. As shown in the following section, this range will translate to a minimal change in the diameter of the beam at the lens.

3.2.2. Aperture to Lens

Now we analyze how the beam propagates out of the aperture and up to the lens. As the laser passes through the flat mirror, it begins to expand again. From Gaussian beam properties found in [13, 14] we can determine how the beam diameter changes as it propagates in free space.

Let's begin this calculation by defining the flat mirror to be at $z=0$. We have determined in the previous section that at the other mirror, $z=-91\text{cm}$, the radius of curvature is $R(z=-91\text{cm})=5\text{m}$ and the diameter of the beam is 0.988mm. A Gaussian beam is symmetric about its beam waist. This means that at $z=91\text{cm}$, the radius and diameter will be the same as it is on the spherical mirror. Now we proceed by calculating the complex radius of curvature at $z=z_0=91\text{cm}$.

$$\frac{1}{q(z = z_0)} = \frac{1}{R(z = z_0)} - i \frac{\lambda}{\pi w^2(z = z_0)} \quad (3.4)$$

$$q(z = z_0) = 3.904 + 2.069i$$

As a Gaussian beam is free to propagate in space, the complex radius of curvature will change as determined by the fundamental propagation law. This law states that as the beam travels a certain distance the complex radius of curvature will increase by that

amount. So we need to determine the distance between the flat mirror and the lens. The distance between the *aperture* and the lens is $L_1=152.4\text{cm}$ (60inches). For now we assume that the flat mirror is exactly at the aperture. Then we will assume a distance of 11.0cm, as calculated in the previous section, between the mirror and the aperture to see how this will change the beam diameter at the lens.

Now by using the fundamental propagation law the complex radius of curvature changes as

$$\begin{aligned}
 q(z) &= q_0 + z - z_0 \\
 q(z = L_1) &= q(z = z_0) + L_1 - z_0 \\
 q(z = L_1) &= q_0 + 152.4\text{cm} - 91.0\text{cm} \\
 q(z = L_1) &= 4.518 + 2.069i
 \end{aligned}
 \tag{3.5}$$

By applying the formula for the complex radius of curvature at $z=L_1$, a value for half the beam diameter, $w(z=L_1)$, and radius of curvature, $R(z=L_1)$, can be determined

$$\begin{aligned}
 \frac{1}{q(z = L_1)} &= \frac{1}{R(z = L_1)} - j \frac{\lambda}{\pi w^2(z = L_1)} \\
 \frac{1}{4.628 + 2.069i} &= \frac{1}{R(z = L_1)} - j \frac{\lambda}{\pi w^2(z = L_1)}
 \end{aligned}
 \tag{3.6}$$

Finally by equating the real and imaginary parts on both sides we get

$$\begin{aligned}
 w(z = L_1) &= 1.111\text{mm} \\
 R(z = L_1) &= 5.465\text{m}
 \end{aligned}
 \tag{3.7}$$

Knowing these two values of the laser at the lens, $z=L_1$, allows us to proceed and calculate how the beam gets expanded by the lens up to the Lloyd's Mirror.

Now let's go back to Eq. 3.5 and increase L_1 to incorporate a possible distance between the flat mirror and the aperture. Now the complex radius of curvature is

$$\begin{aligned}
q(z = L_1) &= q(z = z_0) + L_1^* - z_0 \\
q(z = L_1) &= q_0 + (152.4cm + 11.0cm) - 91.0cm \\
q(z = L_1) &= 4.628 + 2.069i
\end{aligned} \tag{3.8}$$

Then by repeating a similar analysis we get slightly different values for the radius and the beam diameter

$$\begin{aligned}
w(z = L_1) &= 1.134mm \\
R(z = L_1) &= 5.552m
\end{aligned} \tag{3.9}$$

This change in parameters translates to a percent error of 2.02% in the beam diameter and 1.60% in the radius of curvature. This means that the absolute position of the mirrors inside the cavity is not needed for this calculation. Now that we have the diameter of the beam and the radius of curvature we can proceed and calculate how the beam gets expanded as it travels up to the Lloyd's Mirror.

3.2.3 Lens to Lloyd's Mirror

The Gaussian beam should be expanded so that the amplitude of the electric field incident on both edges of the sample is not significantly different. On one edge the center of the Gaussian will be incident with the amplitude of electric field being E_0 . The beam shall be expanded such that the other edge of the sample will be incident with amplitude of $0.90E_0$ or better.

The lens used in the setup is an UV Achromatic Objective (LMU-15X) with an EFL (effective focal length) of 13mm given by the data sheet of the company. With the beam size at the lens, as determined in the previous section, we can calculate how much the beam will expand, from simple geometry as shown in Figure 3.3.

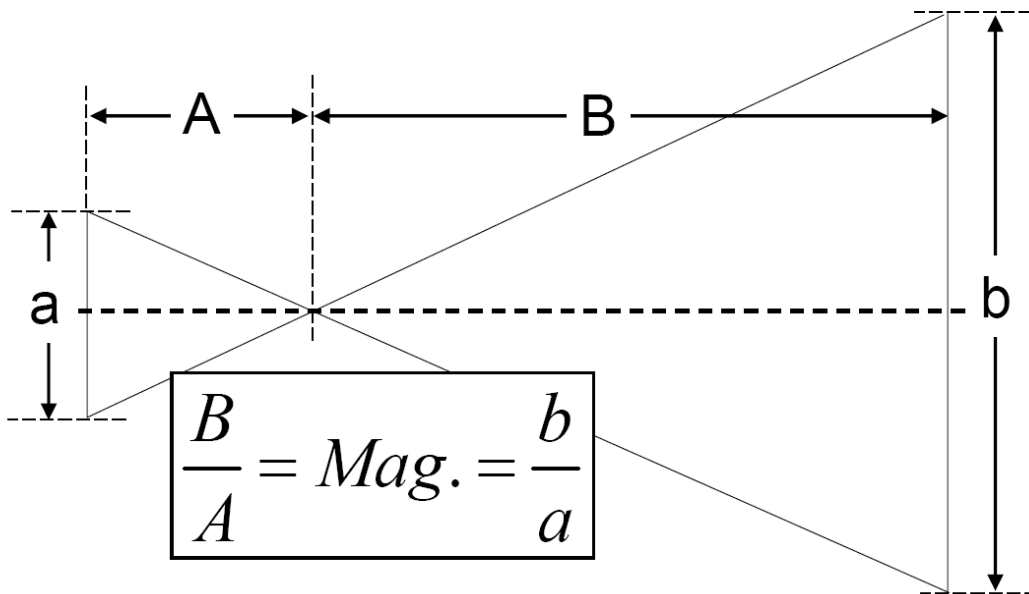


Figure 3.3: Simple geometry helps to determine how much beam expands over distances specified.

$$\frac{w_{Lloyd}}{w(z=L_1)} = \text{Magnification} = \frac{L_2}{f} \quad (3.10)$$

$$w_{Lloyd} = 130.25\text{mm}$$

where $L_2=1524\text{mm}$ is the distance between the lens and the Lloyd's Mirror, f the focal length, $w(z=L_1)$ the beam diameter at the lens, and $w_{Lloyd} = w(L_1 + L_2)$ the beam diameter at the Lloyd's Mirror. Now the profile of the electric field can be plotted at the Lloyd's Mirror for the setup used, Figure 3.4.

The simple geometry used in Eq. (3.10) assumes the lens and the Lloyd's Mirror are in the far field from the focused spot size. As seen in the following section a strong focus will ensure that the lens is in the far field. Furthermore, if the lens is in the far field then so is the Lloyd's Mirror.

The importance behind expanding the beam is to ensure that the amplitude of the electric field incident on the sample is uniform. Expanding the beam translates to a loss in intensity. This loss will simply lead to longer exposure times. One could think that the stability of the system would be a factor by exposing for a longer period of time. This is not a problem with the Lloyd's Mirror setup since only a single beam is used for most of the path traveled. The beam only splits off into two arms at the end when half of the beam reflects off the mirror. Ensuring that the mirror and the sample are connected in a rigid mechanical method will stabilize the system. Only if the mirror moves with respect to the sample will there be any variations.

3.2.4 Pinhole size

Now that we know that the focal length of the lens will expand the beam appropriately, we can calculate the pinhole size needed to filter higher unwanted frequencies. For this t

Electric Field at the Lloyds Mirror

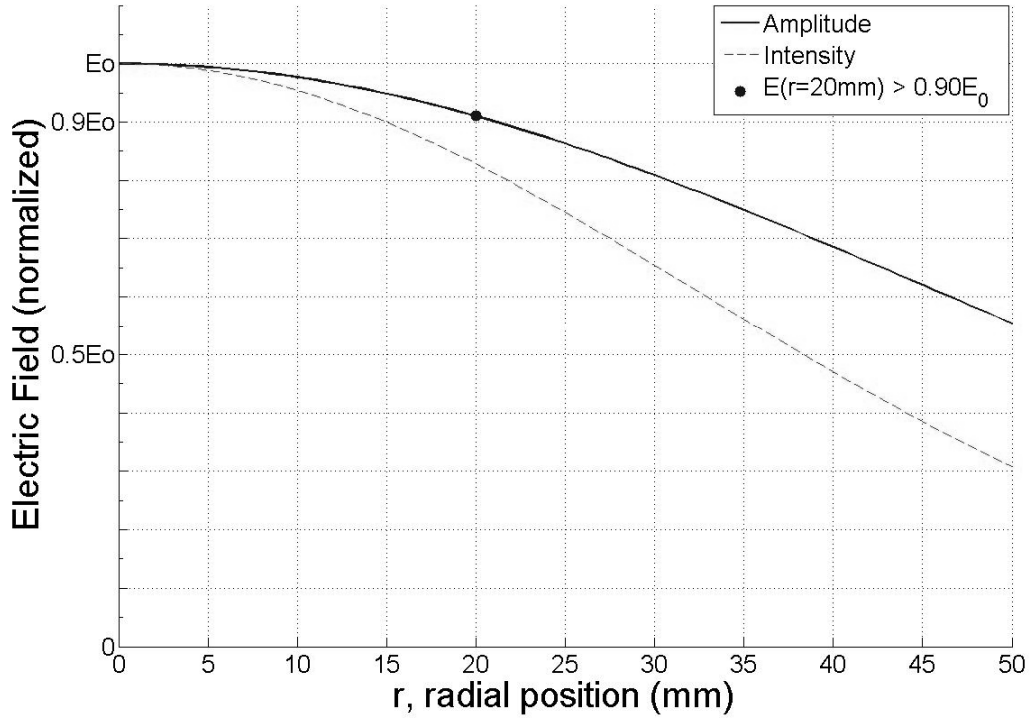


Figure 3.4: The Electric Field at the Lloyd’s Mirror plotted from beam width calculated. Setup has been designed to have amplitude at edge of sample ($r=14.14\text{mm}$) be $0.90E_0$ or higher.

<i>r(radial position)</i>	$5.77\mu\text{m}$	$6.58\mu\text{m}$	$8.16\mu\text{m}$	$8.75\mu\text{m}$	$9.99\mu\text{m}$
<i>E(r), amplitude</i>	$0.10E_0$	$0.05E_0$	$0.01E_0$	$5.0*10^{-3}E_0$	$1.0*10^{-3}E_0$
<i>E²(r), intensity</i>	$0.01I_0$	$2.5*10^{-3}I_0$	$1.0*10^{-4}I_0$	$2.5*10^{-5}I_0$	$1.0*10^{-6}I_0$
<i>pinhole diameter = 2*r</i>	$11.54\mu\text{m}$	$13.16\mu\text{m}$	$16.32\mu\text{m}$	$17.51\mu\text{m}$	$19.99\mu\text{m}$

Table 3.1: Amplitude and Intensity of the HeCd laser ($\lambda=325\text{nm}$) at the beam waist after passing through the UV lens for different radial positions, r .

o be realized we must first calculate the effective diameter of the focused Gaussian spot. From Gaussian beam focusing properties the effective diameter can be found from

$$d_0 = w(L_1 + f) \approx \frac{2f\lambda}{D} \quad (3.11)$$

where $f=13\text{mm}$ is the focal length, $\lambda=325\text{nm}$ the laser wavelength, and

$D = w(z = L_1) = 1.111\text{mm}$ the diameter of the beam before the lens. Plugging all these values into Eq.3.11 gives $d_0 = 5.970\mu\text{m}$.

Recall that $r = w(L_1 + f) = d_0/2$ is where the amplitude of the electric field at the beam waist decays by $1/e$. Similar to the analysis used in Figure 3.4, the amplitude and intensity of the electric field can be determined as a function of radial position. Table 3.1 lists how the amplitude and intensity vary at the waist for different values of r , the radial position.

Placing a pinhole with a diameter of $20\mu\text{m}$ will ensure that nearly all of the beam will pass through. That is, field with amplitude higher than $1.0 \cdot 10^{-3} E_0$ will pass through the pinhole while higher unwanted frequencies or scattering from dust particles will not.

The expression for focused spot size Eq.3.11 assumes a couple of things. First, the Gaussian beam entering the lens is more or less collimated. Recall that the value for the beam diameter and radius of curvature for the Gaussian beam at the lens was calculated in Eq.3.9, $w(L_1) \ll R(L_1)$. Second, the beam is “strongly focused”, i.e. $w(L_1 + f) = d_0/2 \ll w(L_1)$. The second point is equivalent to saying that the lens is in the far field, as seen looking backward from the waist of the focal point. The beam diameter at the lens $w(L_1)$ is so much smaller than the beam diameter at the focus $w(L_1+f)$ that the lens is in the far field. If the lens is in the far field, then so is the Lloyd’s Mirror.

Since both are in the far field, a simple geometric approximation as used in Eq.3.10 is valid to determine how big the beam will be at the Lloyd's Mirror.

3.3. Mirror

When choosing the mirror for the setup realized in this experiment, there are many factors to consider. First, a large mirror would minimize the effects of edge scattering and diffraction and at the same time increase the exposure area. The cost and commercial availability of such a large mirror is a factor that prevents it from being chosen. A BK7 glass, UV protected aluminum mirror with a 2.000" diameter and 0.375" thickness was chosen as the Lloyd's Mirror. It has a $\lambda/10$ surface flatness and a reflectivity of better than 90% at $\lambda=325\text{nm}$. The reflectivity of aluminum at this wavelength remains the same for a broad range of angles. This is not the case for different types of metals or a dielectric stack. Dielectric mirrors are another candidate that offers better reflectivity but only at a particular angle. The setup however has been designed with the ability to change the angle of the mirror.

3.3.1. Aligning Lloyd's Mirror

The period of the grating fabricated is directly dependent on the angle of the incident electric field described by Eq.3.1. In order to ensure such simple geometry is valid for this setup, there are two very important alignments to be made at Lloyd's Mirror.

The first is that the mirror and the sample have to make an angle 90° to each other. Misalignment of the mirror will translate to a change in the angle of incidence of electric field, $\Delta\beta$. This change in angle will in turn cause a change in the period of the

gratings. A thorough calculation in [15] shows that this angle offset, $\Delta\beta$, should be somewhat less than the angular accuracy of the rotation stage, $\Delta\theta$. The rotation stage used has an accuracy of about $\Delta\theta \approx 6 \text{ arcmin}$ or 1.75 mrad . This means $\Delta\beta$ should be less than 3 arcmin or 0.873 mrad .

The second alignment is to ensure that the axis I, created by the intersection of the mirror and the sample, and the axis of the rotation stage, R, are aligned. Again an offset in this alignment will translate to a change in the grating period. As mentioned the laser gets focused to a spot, meaning the sample is illuminated from a point source. This point-source illumination is what gives rise to this error. This second alignment would be unnecessary if a perfectly plane-wave was used.

Let's define the distance between the two axes I and R as l_r and the distance between the "point-source" and the axis I, the expansion length, as l_p . As determined in [15] a different analysis shows that l_r should be about

$$l_r < \frac{l_p \Delta\theta}{2} \quad (3.12)$$

The expansion length is also $L_2 = 0.914 \text{ meters}$ and the rotation stage accuracy $\Delta\theta \approx 1.75 \text{ mrad}$. The calculated alignment tolerance for the distance between axes should then be about 0.8 mm . By designing adaptive plates to be machined, this desired accuracy is met by machinist in the shop.

3.3.2. Angle Calibration

As discussed in the previous section the placement of the Lloyd's Mirror should be realized with accuracy when considering the two alignments mentioned. This will

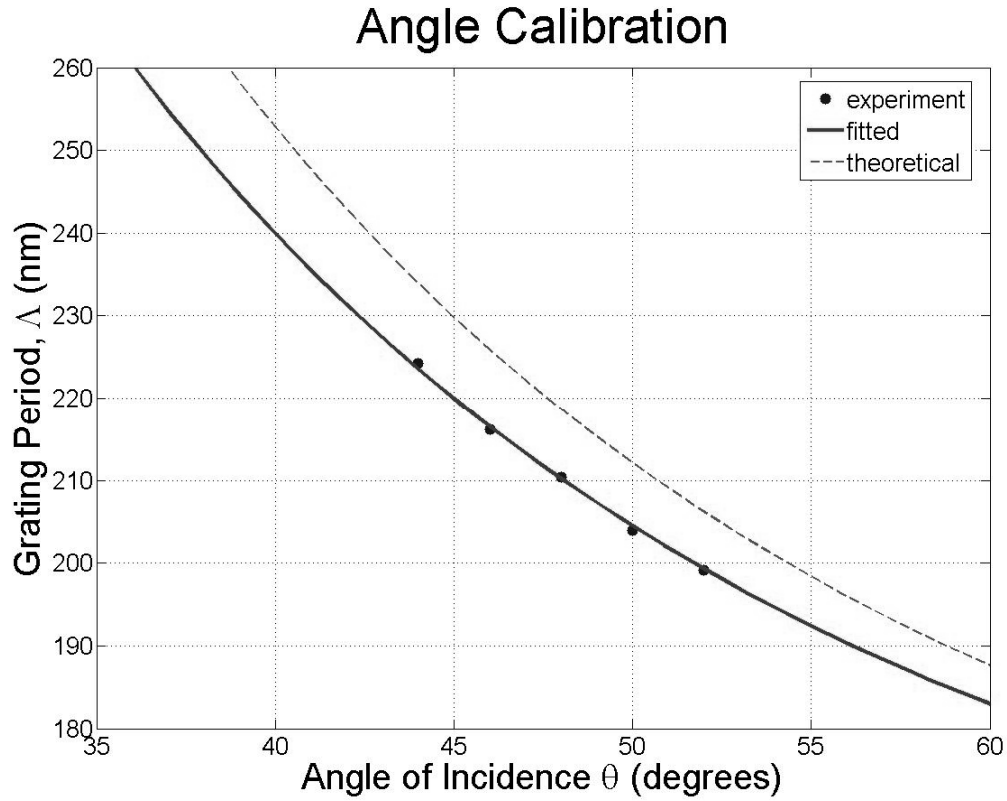


Figure 3.5: Angle Calibration of the Lloyd’s Mirror. The grating period was measured used the alternate setup described in Section 3.5. There is an offset of 2.63° between the fitted and experimental. The fitted curve can be used to determine which angle to use in the setup for a particular grating period desired.

minimize the systematic error related to the angle of incidence for the setup. The most important parameter however is the accuracy of the rotation stage, $\Delta\theta$. If the angular errors from misalignment are less than $\Delta\theta$ then they will not be noticeable. When dealing with the beam, a point source has been used to approximate its behavior meaning its location with respect to the Lloyd's Mirror is irrelevant. Since the beam is actually a Gaussian beam, a simple alignment needs to be made to ensure the center of the Gaussian is incident the center of where the sample and the mirror meet. This can be done by aligning the beam to that spot without the spatial filter.

Any angular errors that arise from misalignment of the mirror can be resolved by a simple angle calibration. This calibration actually ends up being more important than the two mentioned alignments. When setting up the Lloyd's Mirror, there is no easy way to know that the angle on the rotation stage will be the same as the incident angle of the electric field. An angle calibration should tell us what angle to use to achieve a particular grating period. Figure 3.5 shows the ability of this setup to make gratings. An offset of 2.63° exists between the fitted curve and the theoretical equivalent.

In section 2.1.1, the grating period needed to achieve a working wavelength of 1550nm was calculated to be 244.5nm. Now with the calibration realized here, the angle of incidence can be calculated to be 39.0° .

3.3.3. Range of angles

The Lloyd's Mirror setup has been designed so the grating period can be altered by changing the angle of the rotation stage. There is a limit to this range however and can be determined by simple geometry of the setup. As mentioned previously, this

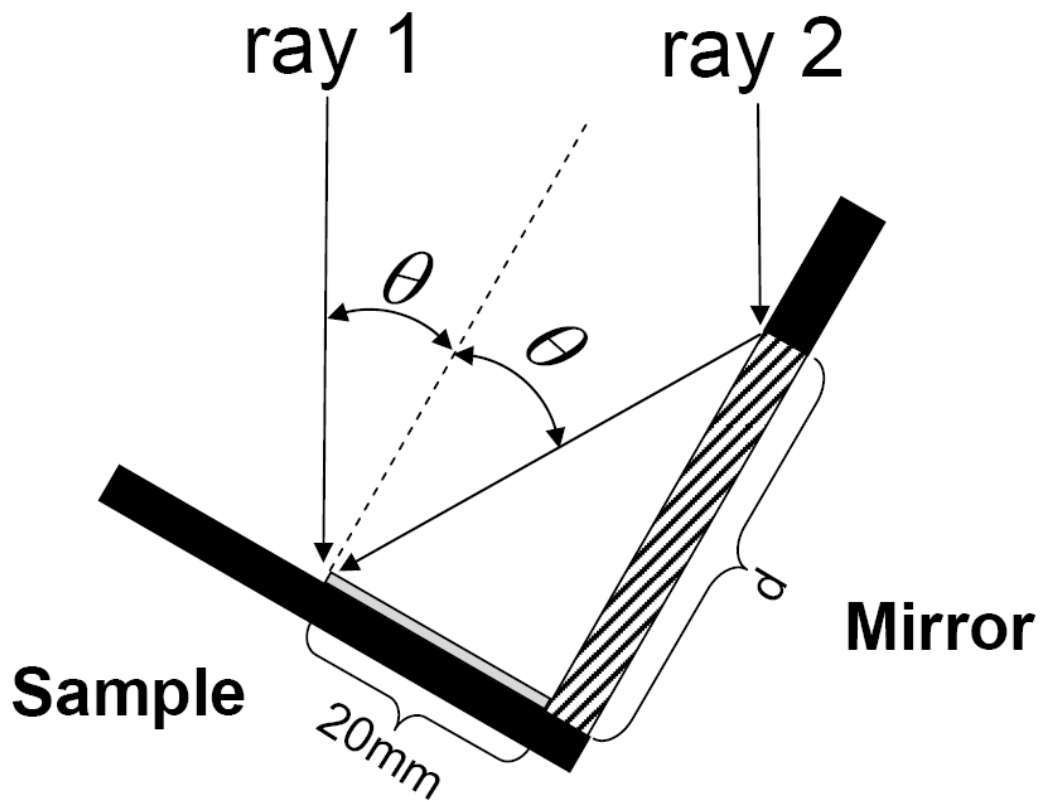


Figure 3.6: Closer look at Lloyd's Mirror. Setup has been designed to ensure that the sample and the mirror have minimal spacing in between the two. This hides part of the mirror making it only $d=40\text{mm}$ from sample to edge of mirror.

experiment has been designed to expose samples as big as 20mm by 20mm. The outermost edge of the two half beams interfere at the edge of the sample, shown in Figure 3.5. From these two vectors is how the range of angles for which this setup works can be calculated.

Figure 3.5 actually shows the *lower* limit of the setup. That is, for any angle of incidence bigger than the one shown, and the setup will still work. The two rays that describe the edge of the beam (ray1 and ray2) can still reflect off the mirror and interfere appropriately at the sample. On the contrary a smaller angle of incidence will result in part of the beam of ray 2 to be reflected off the mirror and part of ray 2 to reflect off the mirror holder. This will result in the two rays to not interfere appropriately. Thus we can calculate the lowest angle of incidence, θ from geometry as described by

$$\tan(\theta) = \frac{20mm}{d} \quad (3.13)$$

where d is the size of the mirror for a particular angle of incidence. Though we have a value for the diameter of the mirror (2inches \approx 50mm) the design hides part of it, and the size gets reduced to 40mm. By plugging in these values the lower bound for the range of angles is approximately 30° . As for the upper bound, no limit can be set unless 90° for which the beam would be incident on the side of the sample and no gratings are made.

3.4. Variation across Sample

3.4.1. Intensity of Electric Field

At first one may think that the intensity of the electric field of the two beams interfering on the sample have to be the same. To better understand the importance of the intensity of the two interfering beams, let's look at contrast, defined in [15] as

Interference contrast for beams of unequal intensity

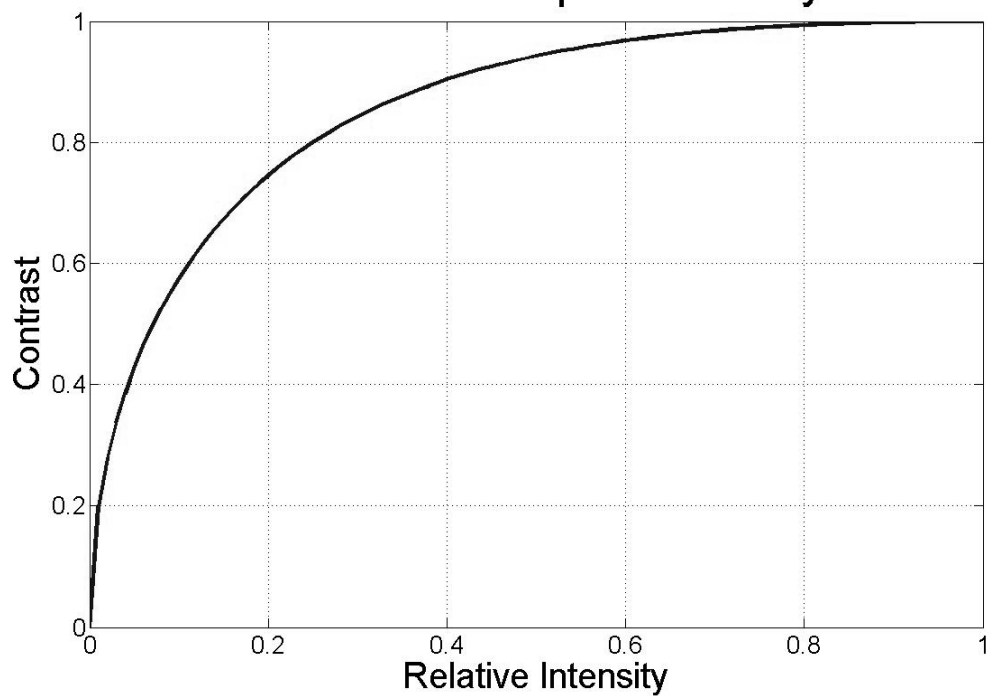


Figure 3.7: Contrast as described 3.4.1 is exactly 1 when the two beams are of equal intensity. As the relative intensity decreases however contrast is lost at a forgiving rate.

$$V = \frac{I_{\max} - I_{\min}}{I_{\max} + I_{\min}} \quad (3.14)$$

Consider the intensity of two different sinusoidal waves. The first has the minima at zero intensity and a maximum to twice the average intensity. The second has higher minima and lower maxima while its average intensity is the same as the first. The first wave will therefore have a higher contrast than the first.

Figure 3.7 shows that two waves with electric fields parallel to each other as considered in this experiment will have a favorable contrast as plotted against their relative intensity. When the two beams have same intensity the contrast will be at its maximum as expected. In the other extreme, contrast reaches zero as the relative intensity goes to zero. However high contrast is still preserved as the relative intensity reaches a mediocre level.

As mentioned in the beginning of Section 3.3, the mirror used has a reflectivity better than 90% at the wavelength used. From the analysis made in this section, such a loss from the mirror can be afforded without any major loss in contrast. Also the distance between the mirror and the sample is minimal compared to the distance the beam travels from the spatial filter to the Lloyd's Mirror. So as the beam reflects off the mirror it travels a minimal distance to the sample and the intensity changes. This small change however is not significant to make a noticeable difference in contrast.

3.4.2. Grating Period

As discussed previously the Gaussian beam is expanded over a length of $L_2=1524\text{mm}$. Essentially a point source is being used located at the pinhole of the spatial filter. This means the beam incident on one side of the sample is incident at a different angle than the

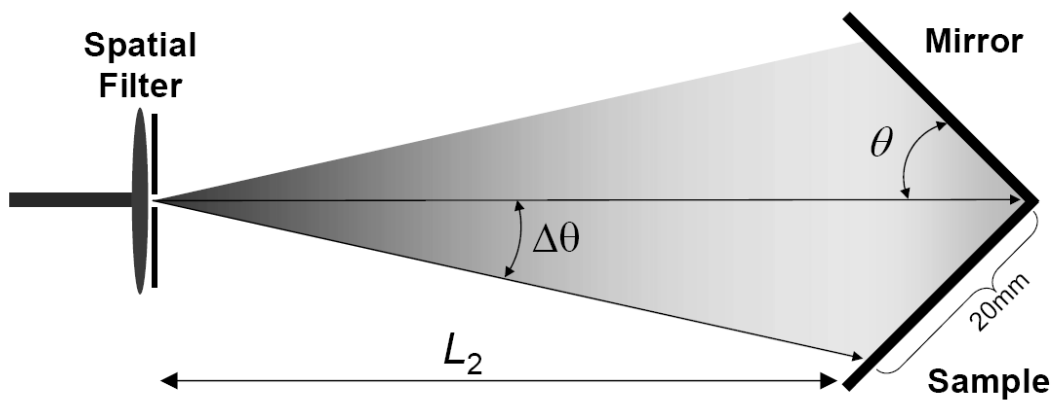


Figure 3.8: A difference in angle $\Delta\theta$ exists between the two beams incident the opposite edges of the sample.

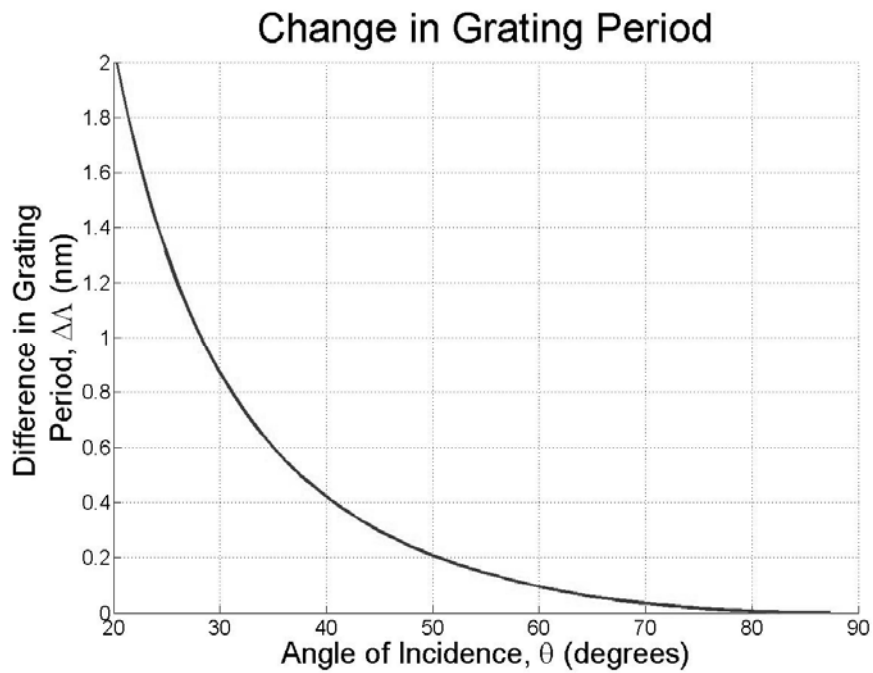


Figure 3.9: The angles of the two interfering beams change across the sample. This translates to a small change in grating period for different angles of incidence.

other. There exists a $\Delta\theta$ between the two beams incident the different edges of the sample (Figure 3.8). This $\Delta\theta$ translates to a variation in angle of incidence across the sample. Using geometry a value for this change in angle can be calculated for different angles of incidence.

$$\begin{aligned}\tan \Delta\theta &= \frac{(20\text{mm})\cos\theta}{L_2} \\ \Delta\theta &= \tan^{-1}\left(\frac{(20\text{mm})\cos\theta}{L_2}\right)\end{aligned}\tag{3.15}$$

This $\Delta\theta$ then in turn translates to a change in angle of incidence. This change in angle of incidence consequently changes the period of the gratings across the sample. The difference in period between the two sides of the sample can be calculated by incorporating this angle difference in the angle of calibration equation. As shown in Figure 3.9, this difference is less than 1nm within the range of angles this setup has been designed for.

3.5. Grating Period Measurement

3.5.1. Alternate Setup

The setup realized in this experiment also allows the user to check the periodicity of the gratings fabricated as demonstrated in [16]. In order to calibrate the setup as was performed in section 3.2.2. Angle Calibration this alternate setup was used to measure how the period changes for samples that had been exposed at different angles of incidence. With the addition of some new elements, the beam of the laser passes through the shutter, a turning mirror, and only one iris diaphragm. Before getting to the second iris, the sample with gratings on top is placed in front of the laser as if it were a turning

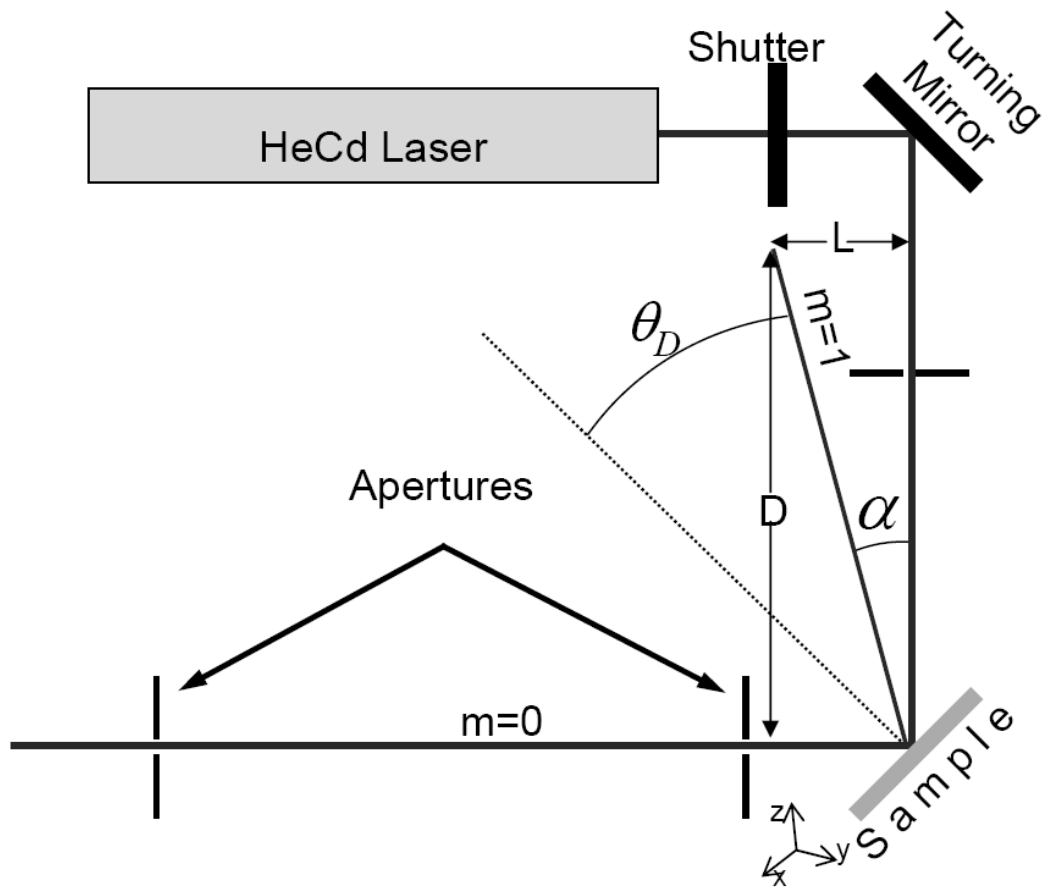


Figure 3.10: The alternate setup also allows the user to check the periodicity of the gratings. This is done by measuring the angle of the diffracted beam, θ_D , and using the relation for the diffraction angle to calculate the period.

mirror. The laser is then redirected through another two apertures to ensure that the angle of the reflected beam is 90° to the incident beam as shown in Figure 3.10. The diffracted angle θ_D can be determined using simple geometry.

$$\begin{aligned}\tan \alpha &= \frac{L}{D} \\ \alpha &= \tan^{-1} \frac{L}{D} \\ \theta_D &= \frac{\pi}{4} - \tan^{-1} \frac{L}{D}\end{aligned}\tag{3.16}$$

Now that the diffracted angle is known, the grating period can be determined from the grating formula

$$\Lambda(\sin \theta_{in} + \sin \theta_{out}) = m\lambda\tag{3.17}$$

where L is the grating period and θ_{in} and θ_{out} are the angle of the beams incident to the gratings and reflected to the gratings, respectively. Note that the angles are defined from the axis perpendicular to the gratings. That is if we look at the $m=0$ beam

$$\begin{aligned}\Lambda(\sin \theta_{in} + \sin \theta_{out}) &= 0 \\ \sin \frac{\pi}{4} + \sin \frac{-\pi}{4} &= 0\end{aligned}\tag{3.18}$$

This means that the $m=1$ beam, the diffracted angle θ_D will be defined as a positive angle. Now plugging in all the values for $m=1$ to find θ_D

$$\begin{aligned}\Lambda \left(\sin \frac{\pi}{4} + \sin \theta_D \right) &= 1 * \lambda \\ \theta_D &= \sin^{-1} \left(\frac{\lambda}{\Lambda} - \sin \frac{\pi}{4} \right)\end{aligned}\tag{3.19}$$

by combining Eqs.3.16 and 3.19 an equation can be derived for the grating period in terms of all parameters determined experimentally

$$\Lambda = \frac{\lambda}{\sin \frac{\pi}{4} + \sin \left(\frac{\pi}{4} - \tan^{-1} \frac{L}{D} \right)} \quad (3.20)$$

3.5.2. Limit to Grating Measurement

There is a limit to measuring the grating period with this setup. If we rewrite Eq.3.20 a different equation can be derived for L as a function of Λ , the grating period, and D, the geometric distance of the diffracted beam

$$L = D \tan \left(\frac{\pi}{4} - \sin^{-1} \left(\frac{\lambda}{\Lambda} - \sin \frac{\pi}{4} \right) \right) \quad (3.21)$$

Since we know $\lambda=325\text{nm}$, the laser wavelength, we can plot L as a function of Λ for different values of D as shown in Figure 3.11. The region for which this alternate setup will work exists around the point where all these lines intersect, $\Lambda \approx 230\text{nm}$. That is, the setup will measure the grating period roughly from 200nm to about 260nm. For any grating periods that lay outside this range, the accuracy of the measurements breaks down.

3.5.3. Making a measurement

This alternate setup can be used for two reasons. The first is to simply check to see if there are any gratings on the sample fabricated. That is you place the sample in front of the laser and if a diffracted beam is observed, then there are gratings present on the sample. By moving the sample around you can check to see which region the gratings are covering on your sample.

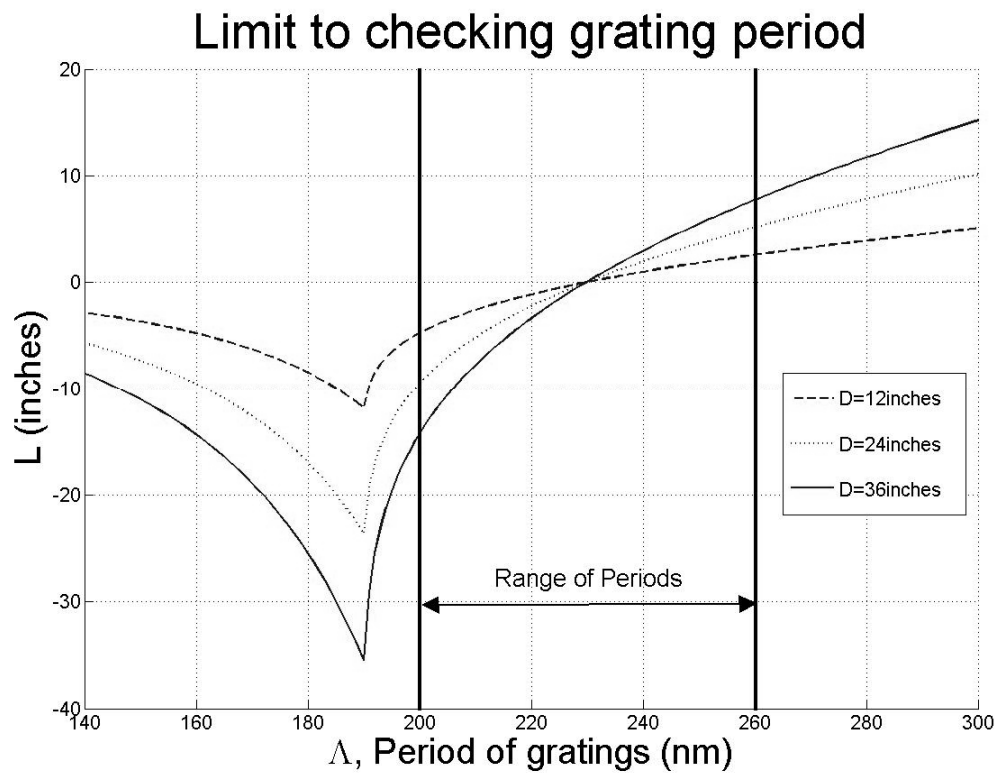


Figure 3.11: The alternate setup used to check the period of the gratings is valid only for a limited range. Gratings with periods outside limited range (200nm-260nm) cannot be measured as accurately

The second reason is to check what the period is on the gratings as mentioned previously. Choosing to check the period requires careful alignment of this alternate setup. First the reflected beam must go through the two apertures. Again, this will ensure that the reflected beam is 90° to the incident beam. If it is not aligned properly, the reflected beam will have an offset, meaning the diffracted beam will have an offset. This offset will translate to an error in the measurement of the diffracted beam angle, which in turn will make an error in the period of the gratings. The second alignment comes from the orientation of the gratings. That is, the gratings must be going perpendicular to the plane of the incident and reflected beam, i.e. the optical table. After aligning the reflected beam through the two apertures, rotating the sample will cause a shift in the diffracted beam. Rotate the sample until the diffracted beam is on the same plane as the incident beam. After both of these careful alignments a measurement can be made to check the period of the gratings.

Chapter 4: Fabrication

In order to get gratings onto semiconductor a procedure is followed involving several steps shown in Figure 4.1. First resist gets spin coated on the sample at the thickness needed. Second it's exposed at the Lloyd's Mirror for a certain amount of time. Third the exposed resist is developed by dipping the sample into a solution developer. Finally the gratings pattern is transferred onto semiconductor by using either a dry etch or a wet etch technique.

4.1. Preparing the Sample

Spin coating resist on top of semiconductor is a standard procedure involving several steps described in Appendix A and B for two different resists. The spin curve for a particular resist will vary depending on its viscosity. All spin curves however behave in the same way in that the faster the spin speed, the thinner the resist becomes.

As mentioned in Section 3.3.2.2 a thickness of 50nm is necessary to avoid unwanted standing wave pattern while exposing. The commercial availability of a positive resist that spins to such a thickness is non-existent. An alternate choice is to dilute the resist with the appropriate solvents. The resist used for this experiment is AZ MiR 701-2DS from AZ Electronic Materials. The solvents are a mixture 15% to 85% of n-Butyl Acetate to EL Thinner by volume. Using these solvents, the resist can be diluted to get the thickness desired plotted in Figure 4.2. By measuring different parts of the sample, the uniformity across the resist can be checked as well shown in Figure 4.3. Methods used to measure the thickness of the resist can be found in Appendix A and B.

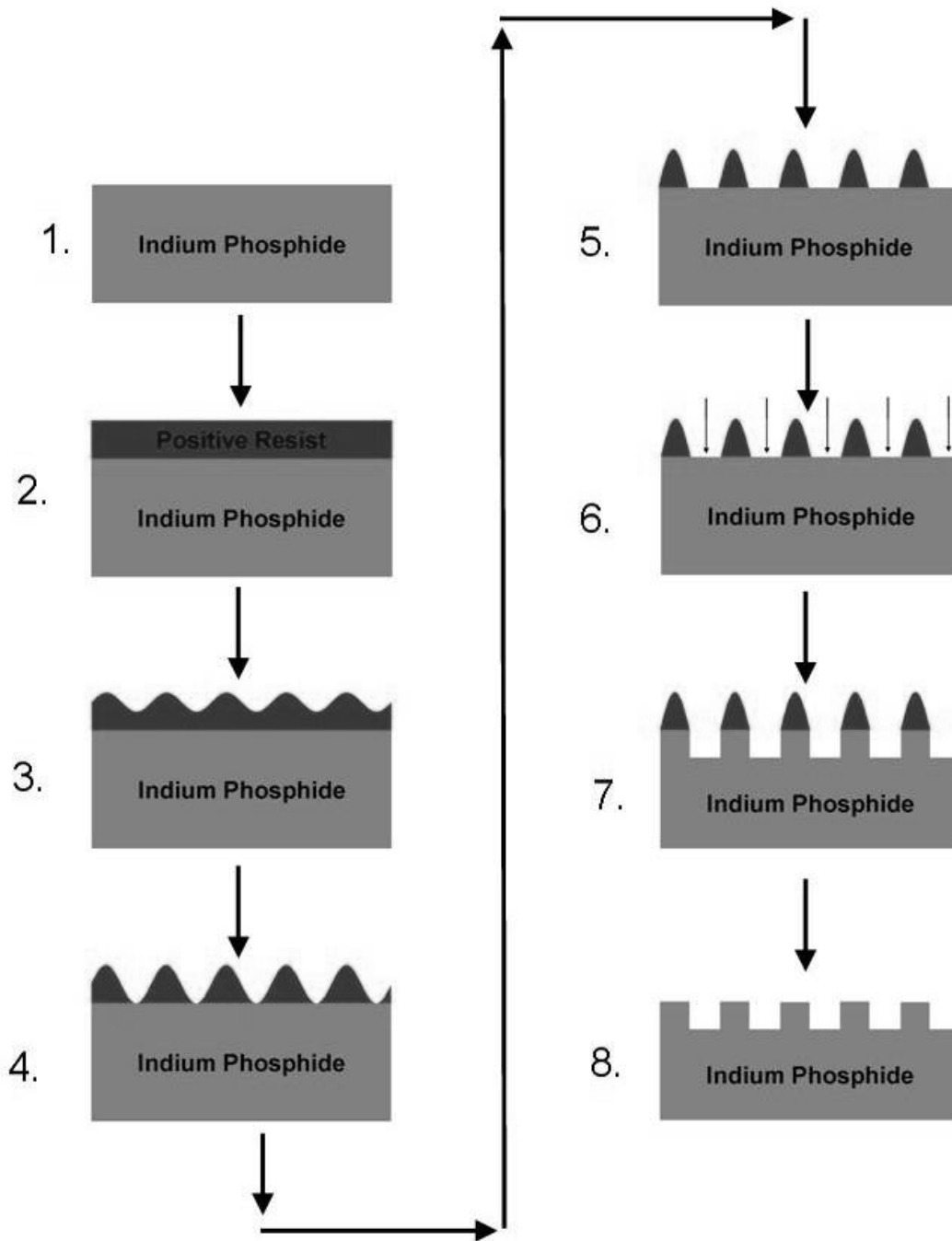


Figure 4.1: Process followed for fabrication of gratings. (1-2)First a thin layer, of Positive Resist is spin coated on top of Indium Phosphide. (3-5)Then sample gets exposed using interference pattern created by UV laser at Lloyd's Mirror. (6-7)Once flat bottoms are achieved, dry etching transfers pattern onto semiconductor. (8)Finally resist is stripped off, leaving behind gratings.

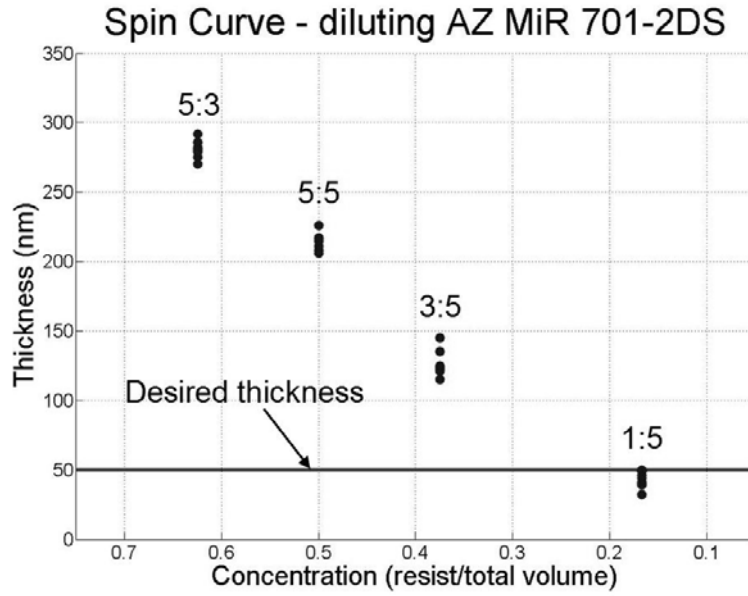


Figure 4.2: By diluting the resist, the desired thickness, 50nm, can be obtained. The concentration of resist to solvent is specified for each set of data. e.g. 3:5::resist:solvent by volume.

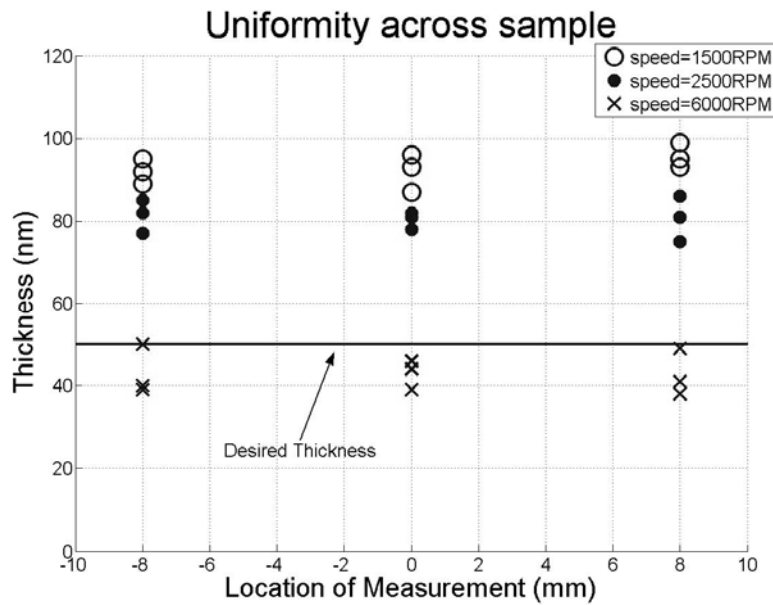


Figure 4.3: By measuring at different spots of the sample, the uniformity of the thickness is observed to be consistent for different spin speeds.

4.2. Exposing Positive Resist using Lloyd's Mirror

After successfully spin coating the resist on top of the semiconductor at the correct thickness, the sample is ready to be exposed. First the laser gets turned on by following proper procedures described in Appendix C. Then the sample is loaded on the holder after making sure both yellow lights only are turned on and that the beam is expanded properly. The beam gets expanded properly by making sure the pinhole in the spatial filter is properly aligned. Finally by using the shutter, the sample gets exposed the appropriate amount of time.

4.2.1. Turning the Laser On

Even before loading the sample for exposure, the laser needs to be turned on. As described in the “Procedures for Operating the HeCd Laser”, found in Appendix C, the laser must remain in any state either on or off for at least 30 minutes. During this wait, part of the processing described above can be realized.

After the laser has reached its steady state, i.e. 30 minutes after turning it on, check the alignment of the beam. Recall all the various elements the laser will pass through before reaching the Lloyd's Mirror. All these elements are essential to ensuring the beam illuminates the sample properly. However the most important is the spatial filter. First allow the beam to pass through without the spatial filter. Then place the UV lens in the appropriate position and ensure the beam expands up to the Lloyd's Mirror. Finally place the correct size pinhole, 20 μ m in diameter, at the beam waist and align to get a clean, smooth beam at the Lloyd's Mirror.

4.2.2. Loading the Sample

After resist has been coated on top of semiconductor, the sample needs to be covered with aluminum foil. This will ensure the resist is unexposed before putting it on the Lloyd's Mirror. Adjust the rotation stage to appropriate angle needed to get the correct grating period. When ready to expose, be sure to turn all room lights off except for the yellow light. The yellow light will aid the user in loading the sample and will not change the properties of the resist.

A timed shutter will ensure the samples get exposed for the correct amount of time. After exposing all samples, rewrap all samples with aluminum foil and take to developing lab.

4.2.3. Getting Flat Bottoms

The required exposure time can be calculated from parameters of the experiment. These are the power density of the laser, the energy density and thickness of the resist. The power density of the laser at the Lloyd's Mirror is measured using a UV detector to be $0.10\text{mWatts}/\text{cm}^2$. The energy density of the resist is a parameter of the material found in its data sheet. For the resist used a value of $190\text{mJoules}/\text{cm}^2\mu\text{m}$ is given for the energy density. With a thickness of 50nm the calculated exposure time is

$$\begin{aligned} \text{Time} &= \frac{\text{EnergyDensity} * \text{thickness}}{\text{PowerDensity}} \\ \text{Time} &= \frac{190\text{mJ} / \mu\text{m} * \text{cm}^2 * (0.050\mu\text{m})}{0.10\text{mWatts} / \text{cm}^2} \\ \text{Time} &= 95\text{sec onds} \end{aligned} \tag{4.1}$$

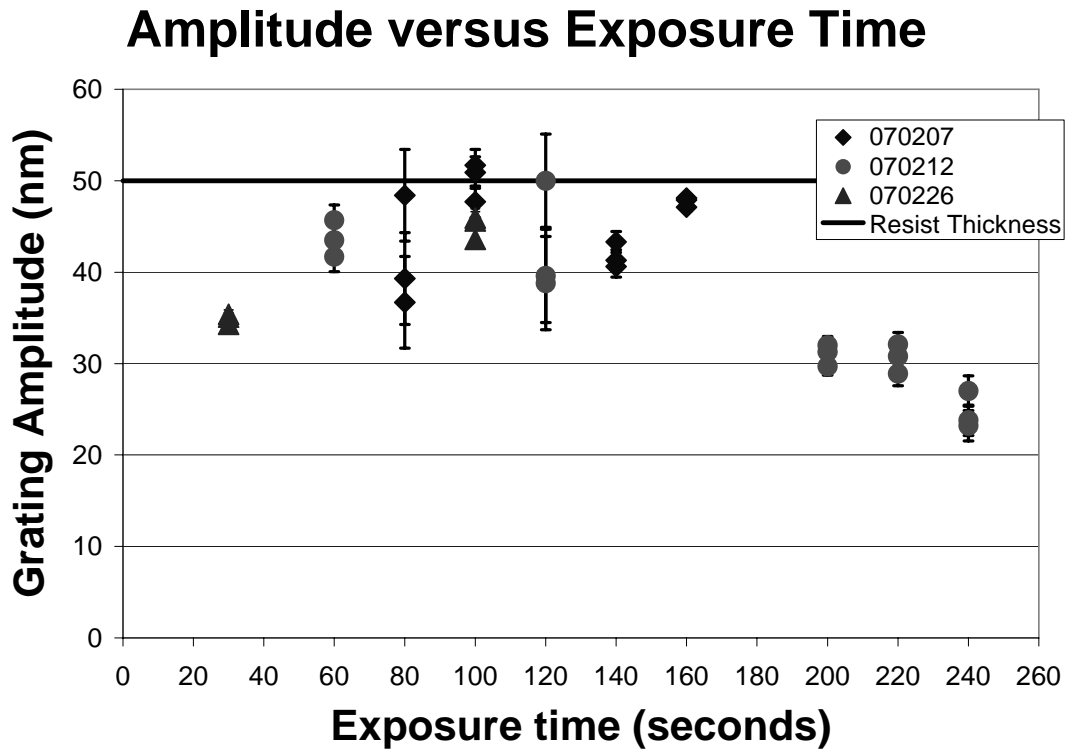


Figure 4.4: Grating amplitude is measured using an AFM and plotted versus the exposure time. The amplitude increases until it peaks around the calculated exposure time where it begins to drop back down for overexposed samples.

This means that if *this* resist at *this* thickness is exposed under or over 95 seconds will be underexposed or overexposed, respectively. For a different resist, the sensitivity will change. Also by varying the thickness this calculated exposure time will also vary. Thus by using the timed shutter, the desired time is input and the sample using this particular resist gets exposed.

Steps 3, 4, and 5 of Figure 4.1, show how the resist evolves as it is exposed for three different times. An underexposed sample, step 3, will have the sinusoidal pattern on top of the resist with part of the resist still being unexposed. In the other extreme, step 5, only the peaks of the sinusoid will remain on the sample when it gets exposed for an extended period of time. Furthermore, the amplitude of the sinusoidal pattern can be measured using an Atomic Force Microscope (AFM) and plotted versus exposure time as shown in Figure 4.4.

Three of the samples used to make amplitude measurements in the AFM were also imaged using a Scanning Electronic Microscope (SEM). The images captured using the AFM give more accurate measurements while the SEM can show the cross section of the sample, qualitatively. The three images captured in Figures 4.5, 4.6, and 4.7, resemble the evolution discussed.

As the sample gets exposed for a longer period of time, the positive resist begins to disappear and only that remains are the top half of the sinusoid and flat bottoms. The top half of the sinusoid is the positive resist while the flat bottoms are the semiconductor being uncovered. Now that the semiconductor is in the open, the next step is to etch the pattern into it.

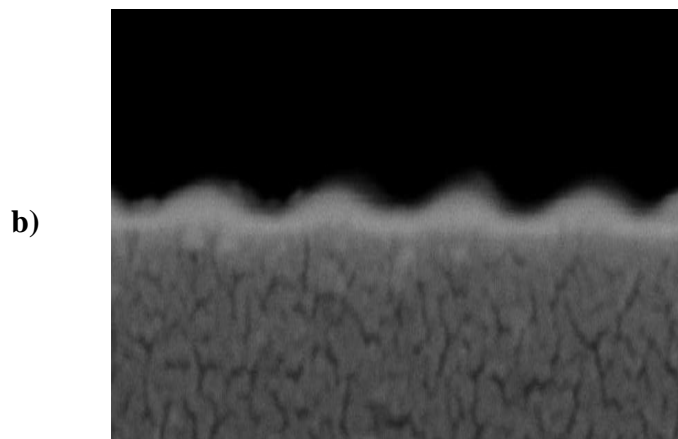
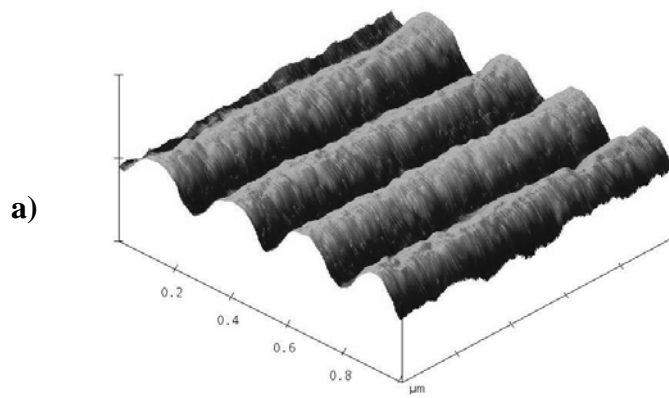


Figure 4.5: Resist exposed at Lloyd's Mirror for 30seconds. a) AFM scan is used to measure the amplitude peak to peak of 35nm while b) SEM scan can be used to qualitatively see the unexposed resist on top of semiconductor material.

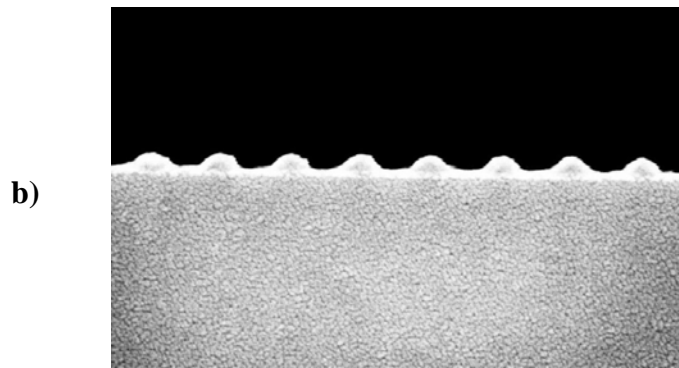
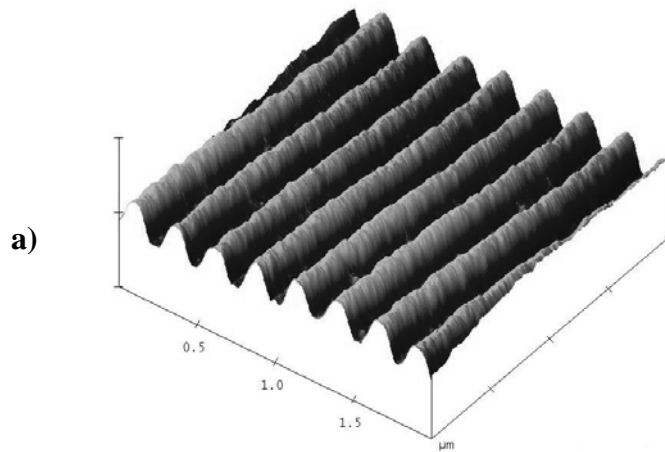


Figure 4.6: Resist exposed at Lloyd's Mirror for 80seconds. a) AFM scan measures an amplitude of 48.4nm while b) SEM scan shows cross section of resist.

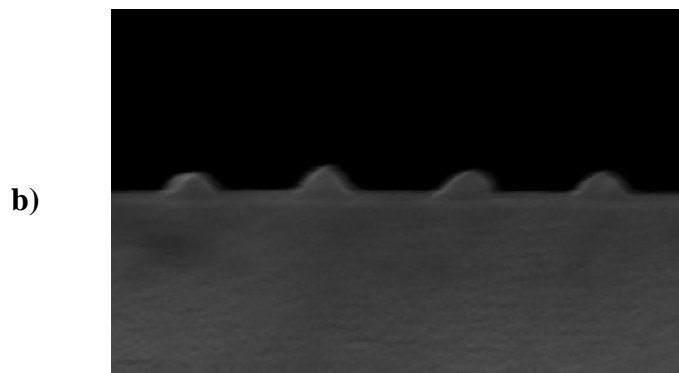
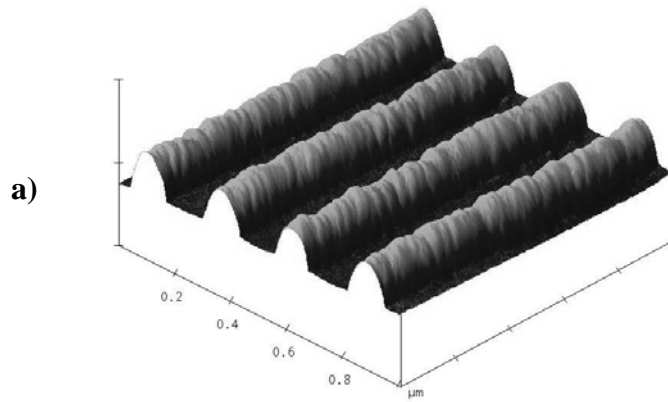


Figure 4.7: Resist exposed at Lloyd's Mirror for 160seconds. a) AFM scan measures the peak-to-bottom of 41.3nm while b) SEM scan shows the semiconductor.

4.3. Etching Gratings into Semiconductor

After developing the sample, gratings are present on positive resist sitting on top of the semiconductor. In order to transfer this pattern into semiconductor either a wet etch recipe or a dry etch recipe can be used. For completeness, both were used here in order to compare their efficiency.

Etching patterns onto semiconductor is a challenging task. There exist a number of recipes that will vary for different semiconductor materials and photo-resistant material. Here a simple overview of the recipes used is presented. An entire different paper can be written on the science and techniques used for etching such materials.

4.3.1. Dry Etch Recipe

A dry etching recipe for Indium Phosphide (InP) is used in the Reactive Ion Etching (RIE). The recipe consists of Methane (CH₄), Hydrogen (H₂), and Argon (Ar) gases and has an etch rate of 500Å/min=50nm/min fully described in [17].

Two samples etched for 60seconds and 120seconds are presented in Figure 4.8 and 4.9, respectively. Using the AFM again, the amplitude of the gratings can be measured. The first sample is measured to have amplitude of 46.1nm and the second sample almost twice the first at 91.3nm. Similar structures are presented using the SEM.

As can be seen on all the scans of the two samples, a “grass-like” structure is present in between the troughs. This is a problem that had been encountered in the past and it comes from a problem in the RIE. Rather than a problem it was a step that had not been taken with this particular sample. That is, the chamber had not been passivated. When this happens small clusters of Aluminum get deposited on the sample and begin to

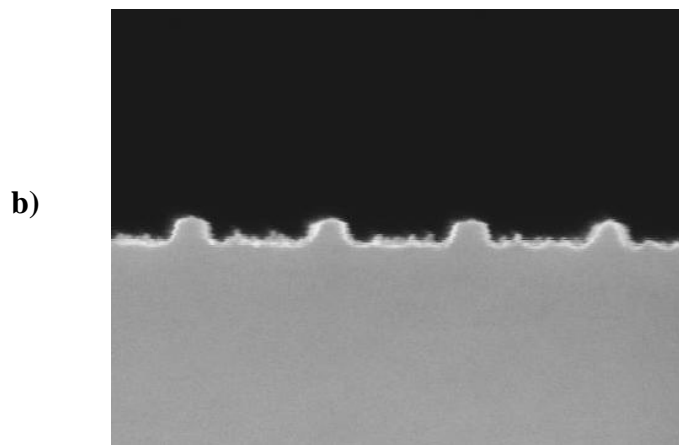
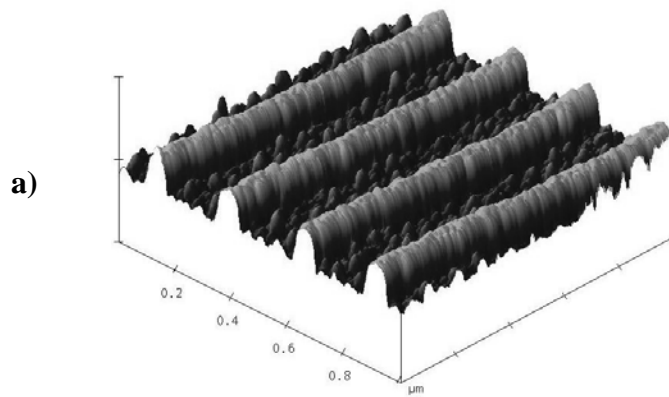


Figure 4.8: Sample exposed at 140seconds is etched for 60seconds. Amplitude of the gratings as measured by the AFM is 46.1nm. SEM scan shows cross section qualitatively.

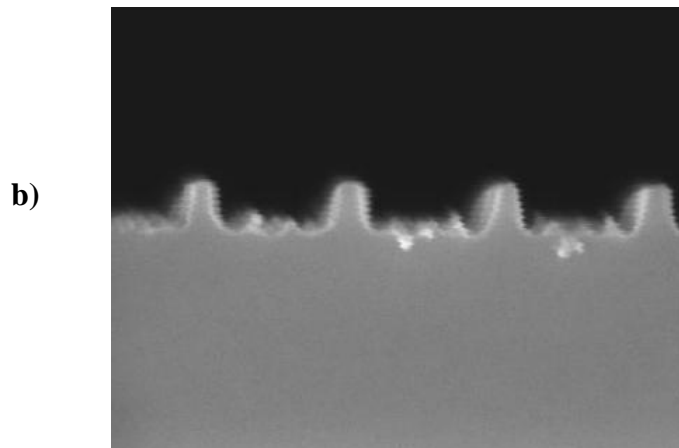
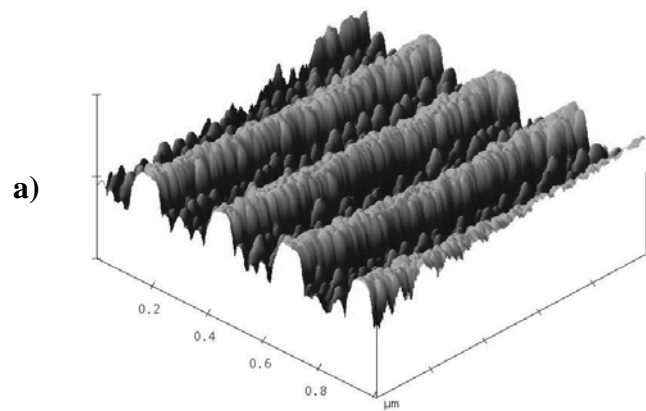


Figure 4.9: Here the sample exposed at 140seconds is etched for 120seconds. Amplitude of the gratings as measured by the AFM is 91.3nm. Again SEM scan shows cross section qualitatively.

act as a mask. Thus when we try to dry etch they would stand on pillars creating this grass like structure [17].

4.3.2. Wet Etch Recipe

After successfully dry etching gratings into Indium Phosphide the experiment took a slight turn. That is, the goal we were after was still the same but at one point the photo-resist we used (AZ MiR 701-2DS) from AZ Electronics had expired. A new type of photo-resist (PR1-2000A) from Futurrex was used and so a completely different recipe was needed as shown in Appendix B. That is, the methodology was still the same for diluting the resist and acquiring the appropriate thickness, but with a different resist comes a different sensitivity and thus a different calculated exposure time.

Figure 4.10 shows an AFM scan of gratings on resist prior to using the wet etch recipe. As shown the gratings that were used for the dry etch recipe has been reproduced with a new photo-resist. Different exposure times are used to compensate for the difference in sensitivity of the resists. Also a different solution from Futurrex is used to develop the exposed material, as described in Appendix B, to leave the unexposed part on top of semiconductor. This new sample very closely assimilates the overexposed sample that was used to get flat bottoms in Figure 4.7.

In order to try a wet etching recipe a different semiconductor material was used, namely Indium Gallium Arsenide (InGaAs). The wet etch recipe for InGaAs consists of dipping the sample into an acid solution. The acid solution mixed here is made up of Phosphoric Acid (H_3PO_4), Hydrogen Peroxide (H_2O_2), and De-Ionized Water (H_2O) with

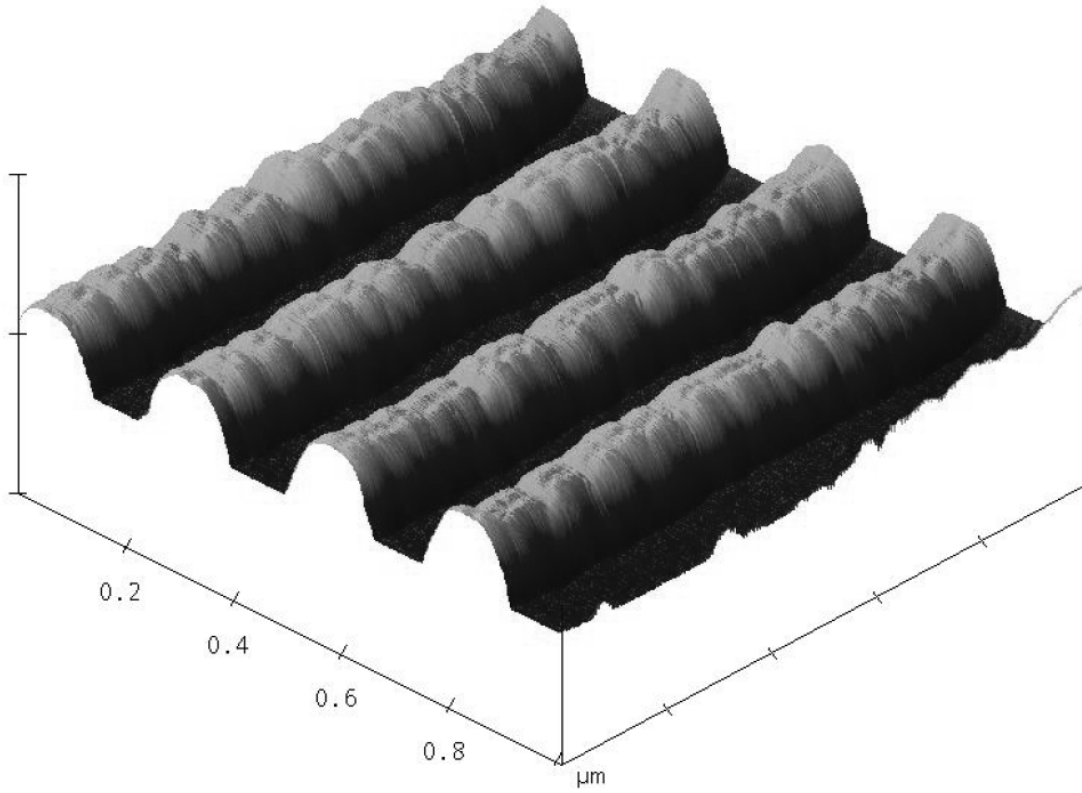


Figure 4.10: With the new photo-resist PR1-2000A we are able to reproduce similar gratings on resist that can be used for etching. This sample resembles that of Figure 4.7 where the sample had been overexposed to get flat bottoms.

proportions specified in Appendix B. The etch rate for this particular recipe is about 12.5nm/sec. This results in a fast dip of 4seconds to etch 50nm into the semiconductor.

Using this recipe, some samples have been dipped for different amounts of time and presented with AFM scans in Figure 4.11. The sample that was dipped for 2 seconds, amplitude measurements of 72.2nm was observed. The 4 second sample has amplitude of 92.9nm. Finally the sample that was dipped for 6 seconds gave amplitude measurements of 116.2nm. Though this last one looks the smoothest, it gave a saw-tooth grating rather than a square wave. This could be from the chemistry of the acid and how it etches into the semiconductor material. Again here only a superficial presentation of etching into this material is presented here. A study of the etch chemistry and ideal recipe is subject of another paper.

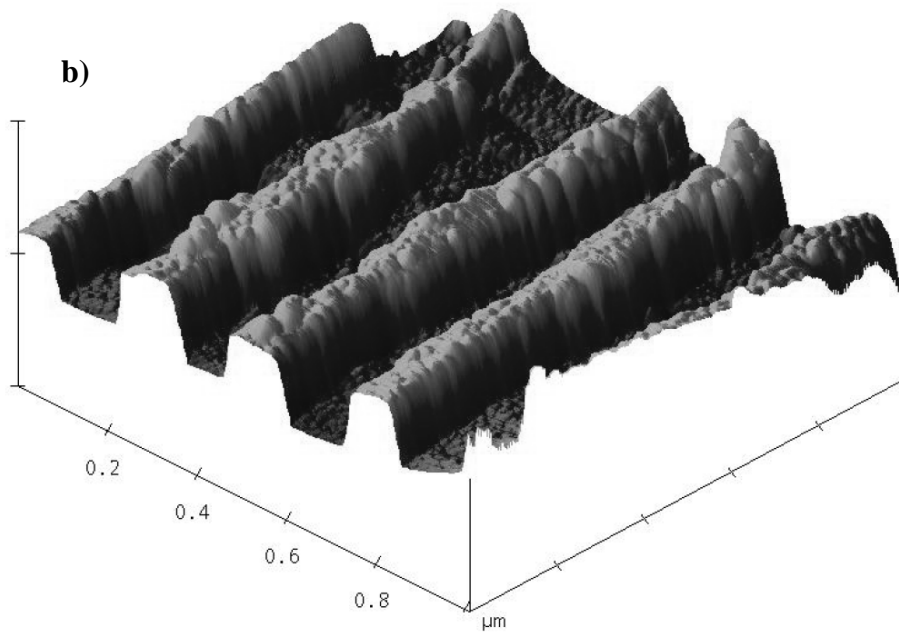
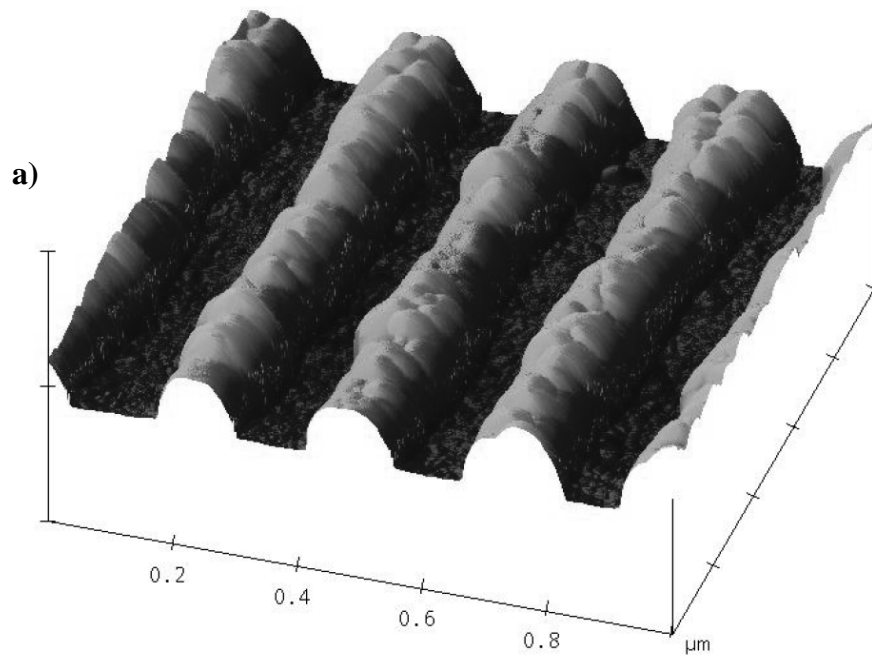


Figure 4.11: Here gratings are wet etched in an acid solution. Samples a and b were etched for 2 and 4 seconds respectively.

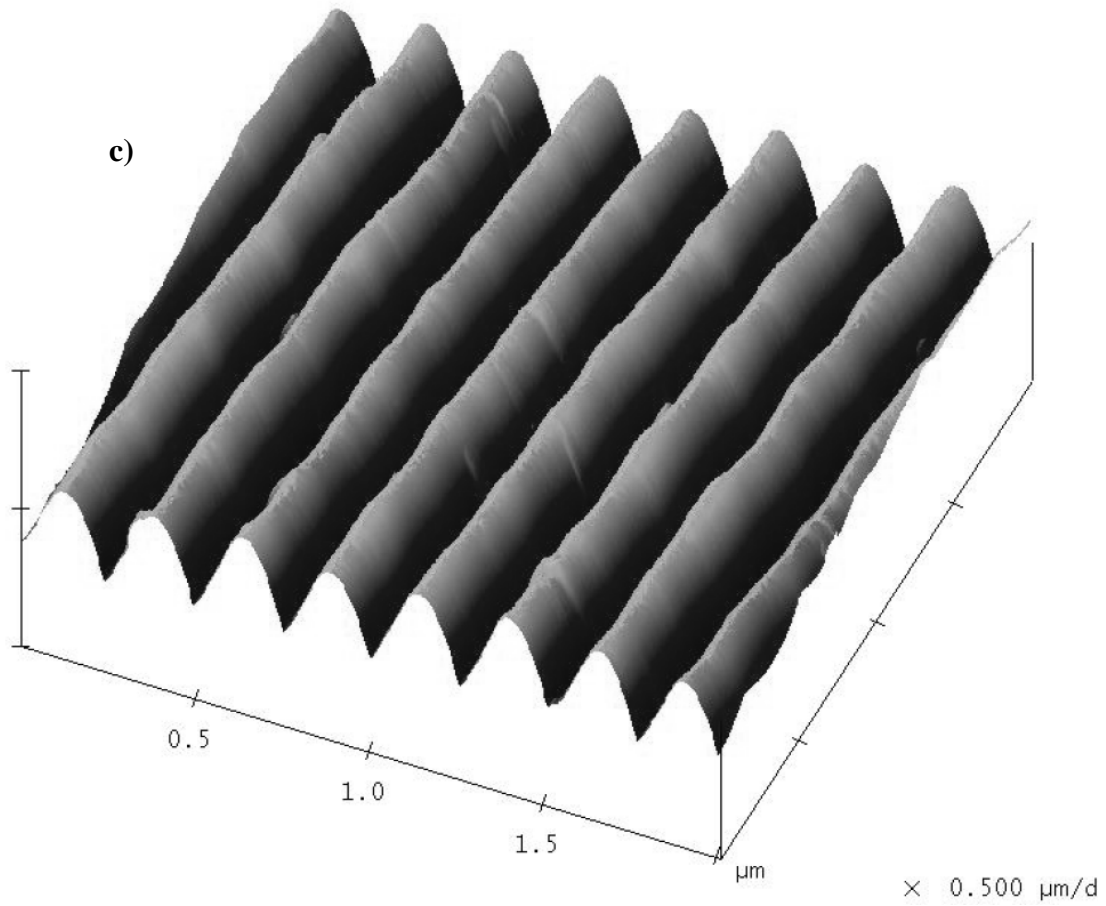


Figure 4.11 (cont'd): Another sample that was wet etched using an acid solution. Here the sample is dipped for 6 seconds and a saw-tooth pattern is observed. This pattern most likely has to do with the chemistry of the acid solution.

Chapter 5: Conclusion

The goal of this thesis being presented was to describe with detail all the work that went into this project. This project set out with the intention of designing a robust setup to fabricate gratings. The work realized here was not to advance the field of Bragg Gratings but to build a setup that would routinely make them. With this setup we will be able to incorporate gratings into waveguides and fabricate DFB lasers at the telecommunication wavelength.

In Chapter 2, I first laid out the theory behind how Gratings work when implemented in a waveguide. When the signal traveling down the waveguide reaches the gratings, it begins to feel a change in the index of refraction. This change caused by the gratings mathematically translates to a sum of small perturbations that create small reflections. Finally these small reflections constructively add to create a signal to be reflected. Secondly I presented a close look at how two plane waves create a standing wave when they interfere. This standing wave will have the period needed for the gratings.

In the following chapter, the setup realized was discussed thoroughly. Since this was the goal of the project most of my time was spent here. Every dimension in the setup was chosen with the idea of making gratings consistently. The Lloyd's Mirror setup provided the most stable way of creating the interference pattern needed. The location and dimensions of the spatial filter was chosen to create an expanded beam that was clean and with minimal variation across the sample. The mirror used for the Lloyd's Mirror was chosen because of its reflectivity at the wavelength and a range of angles. Finally an addition to the setup is presented to measure the period of the gratings fabricated.

Finally in Chapter 4, the process used for fabrication was discussed. First spin coating the resist at the right thickness on top of the sample was the first task. Then by varying exposure times, AFM and SEM scans showed how the gratings evolved. An underexposed sample would have most of the resist still present and a small sinusoid on top. Whereas in an overexposed case the semiconductor is showing as flat bottoms and there is little resist left but the top half of the sinusoid. Finally an etching recipe allows us to transfer this grating pattern on to semiconductor.

Although the setup was designed with the purpose mentioned, alterations can still be made to further investigate Bragg Gratings. A curved mirror would cause chirped gratings which can be studied in the future. The implementation of Bragg Gratings into DFB lasers and DBR lasers will open up the field of study for anyone that gets involved with this project in the future. These Bragg Gratings can serve as a building tool to more advanced topics of research.

Appendix A – Processing Recipes I

==using AZ-MiR 701-2DS==

Step Number	Process Number	Process	Equipment	Specifics/Comments
Gratings Fabrication				
1. Die Preparation				
1	1	Dice	Diamond Scribe	Scribe & Break
2	1	Opticlear rinse	Squirt bottle	15s
3	1	Acetone rinse	Squirt bottle	15s
4	1	Methanol rinse	Squirt bottle	15s
5	1	Isopropanol rinse	Squirt bottle	15s
6	1	Dry	N2 gun	Until dry
7	1	Dry Bake	Hot Plate	90°C-120°C 60s
2. Spin coat Resist				
8	2	Spin HMDS	Spin stand	6000rpm – 1000rpm/s – 60s uncovered
9	2	Spin AZ MiR 701-2DS (1:5 diluted)	Spin stand	6000rpm – 1000rpm/s – 60s covered
10	2	Prebake	Hot Plate	110°C – 60s
11	2	Cover	AL foil	Protect resist from being exposed
3. Expose Positive Resist w/ Lloyd's Mirror				
12	3	Laser on	HeCd Laser	Use proper procedures Appendix B
13	3	Clean Beam	Spatial Filter	Open shutter align pinhole
14	3	Angle of incidence	Rotation stage	Adjust desired angle
15	3	Set shutter time	Timed shutter	Set desired time on shutter
16	3	Expose	Shutter	Yellow light on, load sample, expose desired time
17	3	Cover	AL foil	Re-cover sample to avoid exposure
4. Develop Exposed Resist				
18	4	Develop	Beaker	AZ 300 MiF, 30s
19	4	H ₂ O rinse	Beaker	30s
20	4	Spin dry	Spin stand	2000rpm – 500rpm/s – 60s
5. Dry Etching				
21	5	Prep chamber	RIE 790	Use CR_prep2
22	5	Etch	RIE 790	CR_mha1. stage1(5m): 8sccmCH ₄ + 32sccmH ₂ + 10sccm Ar at 30mTorr 440V DC self-bias; stage2(3m): 16sccm O ₂ at 200mTorr 200V DC self-bias etch rate=50nm/min [17]

Other Useful Procedures				
Test Gratings				
1	TG	Measure diffraction	Alternate Setup	Measure m=1 order as specified section 3.5
2	TG	See diffraction	Beaker w. water	Shine fiber light to see white light get diffracted
3	TG	Grating profile	AFM, SEM	Quantitative and qualitative images to analyze
Diluting Resist				
1	DR	Clean	Dark bottle	Follow process #1 but bake in oven @ 120°C as step 7
2	DR	Mix diluent	beaker	Diluent: 3 : 17 :: n-Butyl Acetate : EL Thinner
3	DR	Dilute resist	Cleaned dark bottle	AZ MiR 701-2DS : diluent :: 1:5
4	DR	Mix diluted resist	stirrer	Using magnetic stirrer mix solution for 300s
Measure Thickness				
1	MT	Spin resist	Spin stand	Follow Process Number 1-2 of Grating Fabrication
2	MT	Expose	Contact aligner	10s exposure using mask that gives features
3	MT	Develop	beaker	Follow Process Number 4 of Grating Fabrication
4	MT	Measure	profilometer	Measure thickness across known feature
5	MT	Strip resist	beaker	Stripper 1165, H ₂ O rinse

Appendix B – Processing Recipes II

==using PR1-2000A==

Step Number	Process Number	Process	Equipment	Specifics/Comments
Gratings Fabrication				
1. Die Preparation				
1	1	Dice	Diamond Scribe	Scribe & Break
2	1	Opticlear rinse	Squirt bottle	15s
3	1	Acetone rinse	Squirt bottle	15s
4	1	Methanol rinse	Squirt bottle	15s
5	1	Isopropanol rinse	Squirt bottle	15s
6	1	Dry	N2 gun	Until dry
7	1	Dry Bake	Hot Plate	90°C-120°C 60s
2. Spin coat Resist				
8	2	Spin HMDS	Spin stand	6000rpm – 1000rpm/s – 60s uncovered
9	2	Spin PR1-2000A (1:10 diluted)	Spin stand	6000rpm – 1000rpm/s – 60s covered
10	2	Prebake	Hot Plate	110°C – 60s
11	2	Cover	AL foil	Protect resist from being exposed
3. Expose Positive Resist w/ Lloyd's Mirror				
12	3	Laser on	HeCd Laser	Use proper procedures Appendix B
13	3	Clean Beam	Spatial Filter	Open shutter align pinhole
14	3	Angle of incidence	Rotation stage	Adjust desired angle
15	3	Set shutter time	Timed shutter	Set desired time on shutter
16	3	Expose	Shutter	Yellow light on, load sample, expose desired time
17	3	Cover	AL foil	Re-cover sample to avoid exposure
4. Develop Exposed Resist				
18	4	Develop	Beaker	RD6 (diluted 2:1), 30s
19	4	H ₂ O rinse	Beaker	30s
20	4	Spin dry	Spin stand	2000rpm – 500rpm/s – 60s
5. Wet Etching				
21	5	Wet Etch	Beaker	H ₃ PO ₄ :H ₂ O ₂ :H ₂ O(1:4:4) mixed by volume, 4-6s
22	5	H ₂ O rinse	Beaker	30s
23	5	Remove resist	wet deck	Steps 3-6 under process 1 (GPC)

Other Useful Procedures				
Test Gratings				
1	TG	Measure diffraction	Alternate Setup	Measure m=1 order as specified section 3.5
2	TG	See diffraction	Beaker w. water	Shine fiber light to see white light get diffracted
3	TG	Grating profile	AFM, SEM	Quantitative and qualitative images to analyze
Diluting Resist				
1	DR	Clean	Dark bottle	Follow process #1 but bake in oven @ 120°C as step 7
2	DR	Mix diluent	beaker	Diluent: 3 : 17 :: n-Butyl Acetate : EL Thinner
3	DR	Dilute resist	Cleaned dark bottle	AZ MiR 701-2DS : diluent :: 1:5
4	DR	Mix diluted resist	stirrer	Using magnetic stirrer mix solution for 300s
Measure Thickness				
1	MT	Spin resist	Spin stand	Follow Process Number 1-2 of Grating Fabrication
2	MT	Expose	Contact aligner	10s exposure using mask that gives features
3	MT	Develop	beaker	Follow Process Number 4 of Grating Fabrication
4	MT	Measure	profilometer	Measure thickness across known feature
5	MT	Strip resist	beaker	Stripper 1165, H ₂ O rinse

Appendix C –Operating the HeCd Laser

Procedures for Operating the Helium Cadmium Laser

NOTE: Each user must read & sign the LPS Standard Operating Procedure (SOP) and be authorized by the Primary Owner (Christopher Richardson)

1. Turn on Laser Warning Light

This is the light that comes on outside the room. Switch located on the wall near door

2. Wear protective goggles

Make sure everyone in the room has appropriate goggles that work for $\lambda=325\text{nm}$ and Optical Density (OD) > 4. Two adequate goggles that work in the range of 190-520nm with OD>9 can be found in a compartment box near the door. Do NOT let people in the room unless they have protective goggles as well.

3. Double check plug connections

Check to make sure the power cables are connected properly and that nothing is loose. Thorough procedures can be found in section 5-4 of Instruction Manual and beginning of Laser Log

4. Turn the laser on

Please follow instructions (5-5 Operation) located near laser/power supply also found in Instruction Manual and Laser Log

5. Write down data in Laser Log

Record: time/date, tube current & voltage. Write appropriate information in the Log along with any necessary notes. Be sure to record any unusual behavior and/or maintenance concerns.

6. 30 minute rule

The laser must be in any state for AT LEAST 30 minutes. That means that you must wait at least 30 minutes before turning the laser off after turning it on. Same goes for when you turn laser back on after having it turned off

7. Turn the laser off after use

You must turn the laser off after usage. Do not leave running overnight.

8. Write down data in Laser Log Part II

Record the time you turned the laser on and off. This will keep track of the # of hours the laser was in operation

9. Cadmium Spill

If for any reason there is a Cadmium leak, you must bring to the Safety Officer's attention for repair and maintenance.

10. Test Data and Instruction Manual

Both the Test Data and the Instruction Manual are located in a white binder in the grey cabinet near the door.

Appendix D - Matlab Code

Here the MATLAB code to solve the effective index of the asymmetric slab. Plot both the RHS and LHS of the transcendental equation and see where they intersect.

```
%%%%%%%%%%%%%%%%%%%%%%%%%%%%%%%%%%%%%%%%%%%%%%%%%%%%%%%%%%%%%%%%%%%%%%%%%%%%%%
%effective index method for asymmetric case w TM modes
%Section I consists of 3 layers to be solved here for air, InGaAs, and
%InP, by varying neff we will be able to solved the transcendental
%equations that specify this problem
%
lambda = 1.55e-6; %telecomm. wavelength of signal
d=100e-9; %thickness in meters of layer in between

n1 = 1; %air
n2 = 3.55; %index for InGaAs
n3 = 3.17;
neff = 2:1e-6:n2; %vary neff to span entire range of indices

k0 = 2*pi/lambda; %wavenumber
beta = k0*neff;
gamma1 = sqrt(beta.^2 - k0^2*n1^2);
k2 = sqrt(k0^2*n2^2 - beta.^2);
gamma3 = sqrt(beta.^2 - k0^2*n3^2);

lhs = tan(k2*d);
top = (gamma1./k2)*(n2^2/n1^2)+(gamma3./k2)*(n2^2/n3^2);
bottom = 1-(gamma1.*gamma3./k2.^2)*(n2^4/n1^2/n3^2);
rhs = top./bottom;

close all;
hold on;
plot(neff,lhs);
plot(neff,rhs,'r');
axis([2 n2 -15 15]);
```

References

- [1] V. Jayaraman, "Extended Tuning Range in Sampled Grating DBR Lasers", *IEEE Photonics Technology Letters*, Vol. 5, No. 5, pp. 489-491 (1993)
- [2] Beck Mason, "Widely Tunable Sample Grating DBR Laser with Integrated Electroabsorption Modulator", *IEEE Photonics Technology Letters*, Vol. 11, No. 6, pp. 638-640 (1999)
- [3] Beck Mason, "Design of Sampled Grating DBR Lasers with Integrated Semiconductor Optical Amplifiers", *IEEE Photonics Technology Letters*, Vol. 12, No. 7, pp. 762-764 (2000)
- [4] W. Feng, "Unselective regrowth of 1.5- μm InGaAsP multiple-quantum-well distributed-feedback buried heterostructure lasers", *Optical Engineering*, Vol. 45, No. 9, pp. 90501-1-3 (2006)
- [5] D. Gollub, "GaInNAs-based distributed feedback laser diodes emitting at 1.5 μm ", *Electronics Letters*, Vol. 40, No. 7, pp. 427-428 (2004)
- [6] Chiu-Lin Yao, "Wavelength-Selectable Lasers With Bragg-Wavelength-Detuned Sampled Grating Reflectors", *Journal of Lightwave Technology*, Vol. 24, No. 9, pp. 3480-3489 (2006)
- [7] D. Schneider, "Wavelength-tunable organic solid-state distributed-feedback laser", *Applied Physics B (Lasers and Optics)*, Vol. B77, No. 4, pp. 399-402 (2003)
- [8] D. E. Aspnes and A. A. Studna, "Dielectric functions and optical parameters of Si, Ge, GaP, GaAs, GaSb, InP, InAs, and InSb from 1.5 to 6.0 eV", *Physical Review B*, Vol. 27, No.2, pp.985-1009 (1983)
- [9] Larry A. Coldren and Scott W. Corzine, "Diode Lasers and Photonic Integrated Circuits", John Wiley & Sons Inc., 1995
- [10] Amnon Yariv, "Optical Electronics in Modern Communications", Fifth Edition, Oxford University Press, 1997
- [11] John David Jackson, "Classical Electrodynamics" Third Edition, John Wiley & Sons, Inc, 1999
- [12] Thomas E. Murphy, "Design, Fabrication and Measurement of Integrated Bragg Grating Optical Filters" in PhD dissertation, Massachusetts Institute of Technology, 2001
- [13] Anthony E. Siegman, "LASERS", University Science Books, 1986

- [14] Javier Alda, “Laser and Gaussian Beam Propagation and Transformation”, Marcel Dekker Inc., 2003
- [15] Mike E. Walsh, “On the design of lithographic interferometers and their applications” in PhD dissertation, Massachusetts Institute of Technology, 2004
- [16] Thomas G. B. Mason, “InP Based Photonic Integrated Circuits”, in PhD dissertation, University of California Santa Barbara, 1999
- [17] Kuldeep Amarnath, “Active Microring and Microdisk Optical Resonator on Indium Phosphide”, in PhD dissertation, University of Maryland, College Park, 2006